Table 2 Morphometric and hemodynamic analyses

	TAC (C57BL/6J, 4 weeks)			PE (C57BL/6J, 7 days)			Ang II (F1/B, 14 days)		
	Sham	TAC	TAC + KB	Vehicle	PE	PE + KB	Vehicle	Ang II	Ang II + KB
	(n = 10)	(n = 9)	(n = 9)	(n = 9)	(n = 9)	(n = 9)	(n = 7)	(n = 7)	(n = 6)
BW (g)	25.2 ± 1.0	24.4 ± 0.9	26.4 ± 0.4	21.7 ± 0.5	20.7 ± 0.3	21.1 ± 0.6	26.9 ± 0.5	26.4 ± 0.6	25.9 ± 0.4
HW (mg)	128.9 ± 12.3	208.3 ± 11.2*	177.7 ± 10.6**	89.9 ± 2.7	100.9 ± 2.1*	91.6 ± 4.0	109.2 ± 3.3	123.0 ± 2.9*	108.8 ± 5.2**
HW/BW (g/mg)	5.09 ± 0.27	8.62 ± 0.56*	6.69 ± 0.35**	4.19 ± 0.07	4.87 ± 0.07*	4.33 ± 0.10**	4.05 ± 0.09	4.67 ± 0.14*	4.20 ± 0.18**
HR (mg^{-1})	644.1 ± 13.7	667.7 ± 13.9	656.1 ± 14.1	502 ± 35	604 ± 31*	578 ± 33	684 ± 36	686 ± 17	648 ± 89
BP (mmHg)	99.4 ± 2.1	101.8 ± 1.7	101.3 ± 4.0	91.2 ± 3.9	115.9 ± 4.5*	118.0 ± 4.8	102.3 ± 2.8	127.7 ± 4.0*	120.0 ± 5.6

KB, KB-R7785; BW, body weight; HW, heart weight; HR, heart rate; BP, blood pressure. Values are means ± s.e.m. *, $P < 0.05$ versus sham or vehicle; **, $P < 0.05$ versus TAC, PE or Ang II.

twice the control level (Fig. 1*e*). KB-R7785 attenuated the increase of [^{3}H]leucine uptake induced by PE, Ang II- and ET-1, whereas stimulation of [^{3}H]leucine uptake by soluble HB-EGF was unaffected. HB-EGF neutralizing antibody also inhibited [^{3}H]leucine uptake. These results are consistent with the hypothesis that EGFR transactivation resulting from the shedding of HB-EGF is a common event in the pathways promoting cardiac hypertrophy.

ADAM12 is involved in GPCR-induced HB-EGF shedding

We used two additional metalloproteinase inhibitors (OSU7-6 and OSU9-6), which showed similar inhibition of HB-EGF shedding but had different inhibitory effects on MMP-1, MMP-3 and MMP-9 (ref. 16). Both OSU7-6 and OSU9-6 caused a similar attenuation of EGFR transactivation by GPCR agonists (Fig. 1*f*), although OSU7-6 was a more potent inhibitor of MMP-1, -3 and -9 than OSU9-6. These results indicated the involvement of other metalloproteinases besides MMP-1, -3 or -9. Next, we identified the specific protease causing HB-EGF shedding in cardiomyocytes. HB-EGF shedding is regulated by protein kinase C (PKC), especially PKC-δ isoform activation[17,18]. We used the yeast two-hybrid method to screen for proteases binding to the PKC-δ regulatory region in a cDNA library constructed from human heart tissue mRNA; this resulted in the identification of ADAM12. Then a plasmid carrying the cDNA of flag-tagged wild-type ADAM12 (WT-ADAM12) or its metalloprotease-domain deleted mutant (ΔMP-ADAM12) was stably transfected into HT1080/HB-AP cells, and the transfectants of WT-ADAM12 (W46 and W48) and ΔMP-ADAM12 (Δ53 and Δ57) were cloned. After the exposure to PE, the secretion of HB-EGF-AP into the culture medium was measured by detecting AP activity. Although the level of HB-EGF-AP expression was similar (Fig. 2*a*), W46 and W48 showed a 1.3–1.5-fold increase of AP activity in the culture medium after

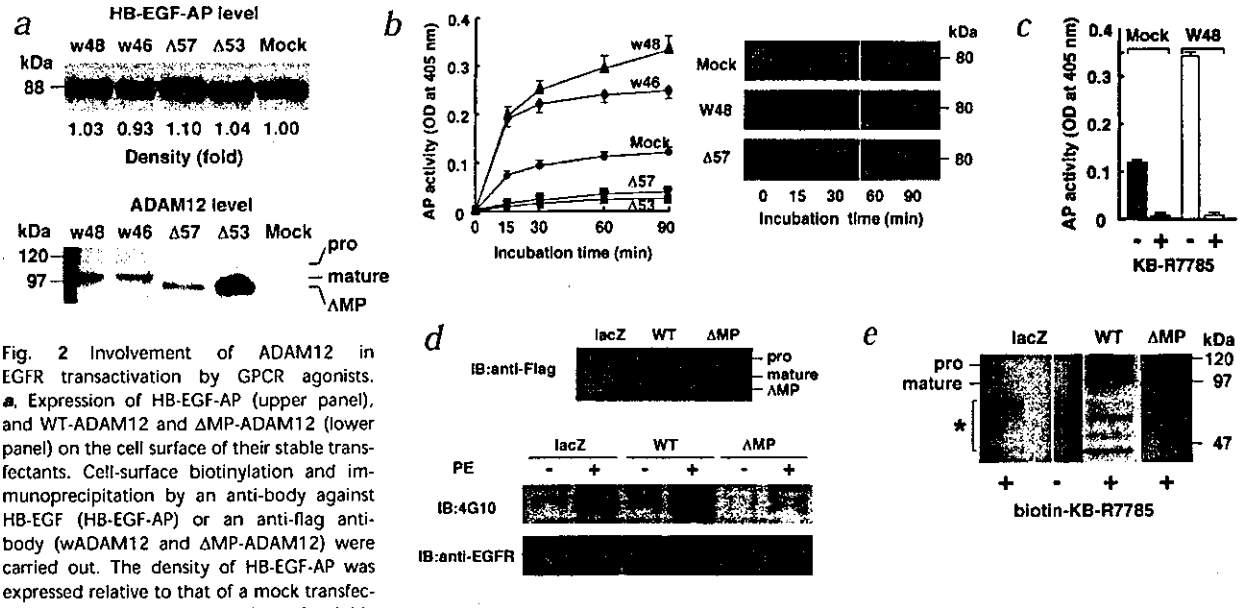

Fig. 2 Involvement of ADAM12 in EGFR transactivation by GPCR agonists. ***a***, Expression of HB-EGF-AP (upper panel), and WT-ADAM12 and ΔMP-ADAM12 (lower panel) on the cell surface of their stable transfectants. Cell-surface biotinylation and immunoprecipitation by an anti-body against HB-EGF (HB-EGF-AP) or an anti-flag antibody (wADAM12 and ΔMP-ADAM12) were carried out. The density of HB-EGF-AP was expressed relative to that of a mock transfectant. ***b***, PE-induced production of soluble HB-EGF-AP activities (left panel) and proteins (right panel) in conditioned media. Each point is the mean of quadruplicate measurements ± s.d. ▲, W48; ◆, W46; ●, mock; ▼, Δ57; ■, Δ53 cells. ***c***, KB-R7785 equally inhibited soluble HB-EGF-AP production induced by phenylephrine in a mock transfectant and W48 cells. ■, mock; □, W48. ***d***, ΔMP-ADAM12 expression blocked EGFR transactivation by phenylephrine in cultured cardiomyocytes. Expression of WT-ADAM12 and ΔMP-ADAM12 in adenovirus-infected cultured cardiomyocytes was shown by western blotting with an anti-flag antibody (upper panel). Immunoprecipitates with the polyclonal antibody against EGFR were immunoblotted with the monoclonal anti-phosphotyrosine antibody 4G10 (middle panel) or with anti-EGFR (lower panel). ***e***, Biotinylated KB-R7785 (biotin-KB-R7785) bound to WT-ADAM12, but not to ΔMP-ADAM12 in cardiomyocytes. *, nonspecific bands of avidin-HRP.

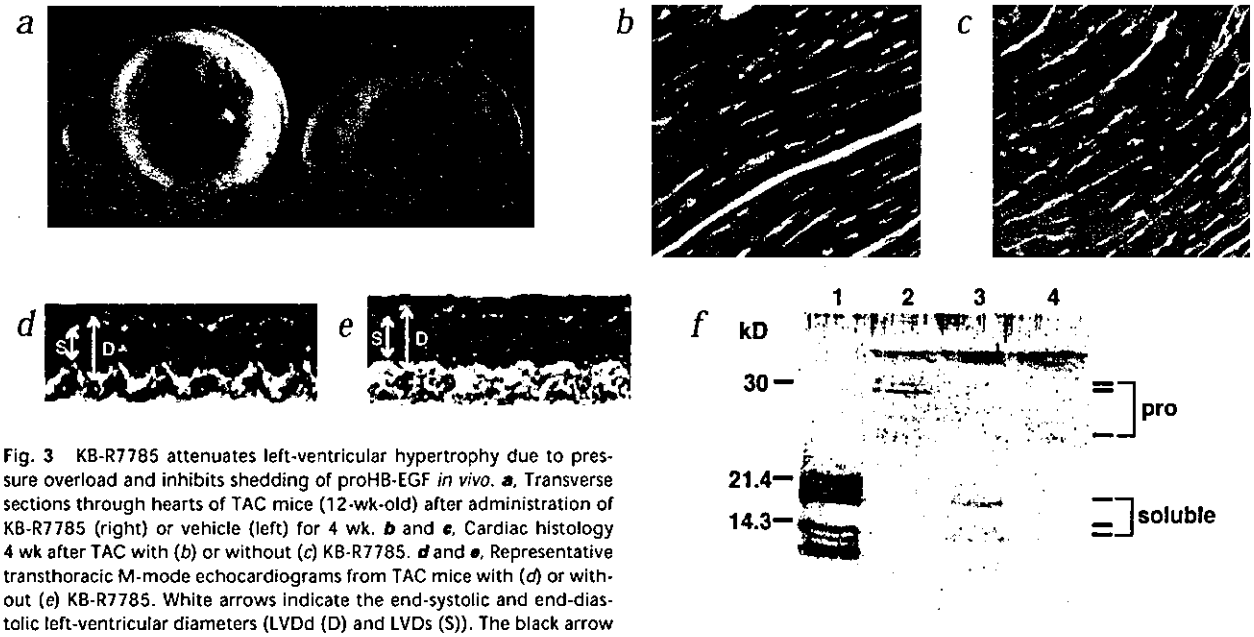

Fig. 3 KB-R7785 attenuates left-ventricular hypertrophy due to pressure overload and inhibits shedding of proHB-EGF *in vivo*. ***a***, Transverse sections through hearts of TAC mice (12-wk-old) after administration of KB-R7785 (right) or vehicle (left) for 4 wk. ***b*** and ***c***, Cardiac histology 4 wk after TAC with (*b*) or without (*c*) KB-R7785. ***d*** and ***e***, Representative transthoracic M-mode echocardiograms from TAC mice with (*d*) or without (*e*) KB-R7785. White arrows indicate the end-systolic and end-diastolic left-ventricular diameters (LVDd (D) and LVDs (S)). The black arrow shows posterior-wall thickness (PWT). ***f***, Detection of HB-EGF protein in mouse hearts by immunoblotting with anti-HB-EGF. Lanes: 1, recombinant soluble HB-EGF; 2, TAC mouse treated with KB-R7785; 3, TAC mouse without KB-R7785 treatment; 4, BL-6 mouse. The heterogeneous bands of soluble HB-EGF and proHB-EGF are derived from multiple N-terminal truncations and heterogeneous sugar chains[22].

90 minutes of PE treatment when compared with mock-transfected cells. In contrast, Δ53 and Δ57 showed 60–70% suppression of AP activity in the medium after PE treatment. AP activity was shown to correspond with the HB-EGF-AP level in the culture medium. A gradual increase of soluble HB-EGF-AP (80 kD) was seen with W48 cells, but was less apparent with Δ57 cells as compared with that of mock cells (Fig. 2*b*). KB-R7785 completely blocked the release of HB-EGF-AP from W48 cells (Fig. 2*c*).

To confirm that endogenous ADAM12 was responsible for the shedding of HB-EGF in cultured cardiomyocytes, we used an adenovirus vector bearing the cDNA of ΔMP-ADAM12 for the analysis of EGFR transactivation by PE. Expression of ΔMP-ADAM12 suppressed EGFR transactivation by PE, whereas overexpression of WT-ADAM12 slightly enhanced EGFR transactivation when compared with LacZ-overexpressing cardiomyocytes (Fig. 2*d*). Direct binding of KB-R7785 to ADAM12 was also confirmed. We transfected adenovirus WT-ADAM12 and ΔMP-ADAM12 to cardiomyocytes and the cells were incubated with biotinylated KB-R7785. Subsequent electrophoresis revealed that biotinylated KB-R7785 showed direct binding to WT-ADAM12, but not to ΔMP-ADAM12 (Fig. 2*e*). These data indicated that, at least in cardiomyocytes, ADAM12 is the specific enzyme of HB-EGF shedding and is a potential target of KB-R7785.

KB-R7785 attenuates pressure overload hypertrophy in mice

Next, we examined the effect of KB-R7785 on cardiac hypertrophy in response to pressure overload on the left ventricle. We subjected mice to thoracic aortic constriction (TAC), which produced a systolic pressure gradient of nearly 45 mmHg between the left and right carotid arteries (right, 90.3 ± 6.5 mmHg; left, 45.8 ± 2.6 mmHg). Pressure overload caused marked thickening of the left-ventricular posterior wall on echocardiography two and four weeks after TAC compared with sham-operated mice (Fig. 3*a*, *c* and *e*). The ratio of heart-weight to body-weight also increased by 69% over that in sham-operated mice at four weeks after TAC. Daily administration of KB-R7785 (100 mg/kg) significantly lessened the increase in left-ventricular wall thickness (2 and 4 wk after TAC) and heart:body-weight ratio (4 wk after TAC) (Tables 2 and 3). KB-R7785 significantly improved fractional shortening four weeks after TAC (Table 3). Both before and after TAC, blood pressure was similar in the mice with and without KB-R7785, suggesting that hemodynamic changes could not explain the beneficial effect of KB-R7785. Histological examination revealed that the reduction of wall thickness by KB-R7785 was due to a decrease of cardiomyocyte diameter, and neither fibrosis nor myofibril degradation was detected in both sham-operated and KB-R7785-treated mice (Fig. 3*a*, *b* and *d*). KB-R7785 also blocked the shedding of HB-EGF *in vivo* since proHB-EGF was detected by western-blot analysis, whereas soluble HB-EGF was predominant in the hearts of untreated mice (Fig. 3*f*).

KB-R7785 attenuates hypertrophy induced by PE or Ang II

We also examined the effect of KB-R7785 on cardiac hypertrophy induced by GPCR agonists (PE and Ang II) in mice with two different genetic backgrounds (C57BL/6J and FVB), since it was unclear whether cardiac hypertrophy was due to the pressure overload model directly mediated through GPCRs. Both PE and Ang II treatment increased heart:body-weight ratio more than 10%. Daily administration of KB-R7785 (100 mg/kg) significantly attenuated the increase of heart:body-weight ratio for both groups (Table 2). The administration of KB-R7785 did not affect blood pressure in either PE- or Ang II-treated mice, suggesting that hemodynamic changes could not explain the effect of KB-R7785. These results confirm our hypothesis that both GPCR-mediated HB-EGF processing and cardiac hypertrophy are blocked by KB-R7785 *in vivo* as well as *in vitro*.

Table 3 Echocardiographic measurements in mice with aortic banding

	0 week			2 weeks			4 weeks		
	Sham (n = 10)	TAC (n = 13)	TAC + KB (n = 10)	Sham (n = 10)	TAC (n = 9)	TAC + KB (n = 9)	Sham (n = 10)	TAC (n = 9)	TAC + KB (n = 9)
PWT (mm)	0.55 ± 0.27	0.54 ± 0.31	0.57 ± 0.29	0.66 ± 0.20	0.87 ± 0.30*	0.69 ± 0.30**	0.66 ± 0.20	1.02 ± 0.33*	0.74 ± 0.12**
EDD (mm)	3.05 ± 0.10	3.06 ± 0.10	3.06 ± 0.09	3.44 ± 0.08	3.05 ± 0.07	3.07 ± 0.15	3.27 ± 0.17	3.24 ± 0.08	3.20 ± 0.15
ESD (mm)	1.98 ± 0.10	1.96 ± 0.08	2.00 ± 0.14	2.23 ± 0.08	1.89 ± 0.08	2.04 ± 1.34	1.94 ± 0.14	2.38 ± 0.10*	2.00 ± 0.15**
FS (%)	35.3 ± 2.5	35.9 ± 2.1	35.4 ± 2.4	35.1 ± 1.4	38.2 ± 1.8	34.3 ± 2.5	40.6 ± 2.5	31.1 ± 1.8*	38.1 ± 2.2**

Echocardiographic measurements obtained from transthoracic M^mode tracings with and without KB-R7785 at 0, 2 and 4 weeks after TAC or sham opereations. PWT, posterior-wall thickness; EDD, end-diastolic diameter; ESD, end-systolic diameter; FS, fractional shortening. Values are means ± s.e.m. *, $P < 0.05$ versus sham; **, $P < 0.05$ versus TAC.

Discussion

We showed that stimulation of cultured rat neonatal cardiomyocytes with PE, Ang II or ET-1 induced the transactivation of EGFR and subsequent increases in protein synthesis after shedding of HB-EGF from the cell surface, based on the complete abrogation of these changes by a neutralizing antibody specific for HB-EGF or a metalloproteinase inhibitor KB-R7785. ADAM12 was identified as the protease causing the shedding of HB-EGF. ADAM12 was also shown to be the target protease for KB-R7785 because of direct binding to this compound, although KB-R7785 may have other effects. The fact that the dominant-negative form of ADAM12 completely abolished the EGFR transactivation induced by a GPCR agonist in cardiomyocytes indicates that, in the heart, ADAM12 is solely involved in this pathway and is also the potential target of KB-R7785. However, because we did not test the dominant-negative forms of other ADAMs or MMPs, we could not completely exclude the possibility of their involvement in the EGFR transactivation induced by a GPCR agonist. Based on the finding that Moss *et al.* successfully cloned a TNF-α shedding enzyme (TACE) from the spleen by specific binding to a metalloproteinase inhibitor (GW9277)[19], and despite the broad spectrum of GW9277 *in vitro*, we suggest that KB-R7785 specifically interacted mainly with ADAM12 in heart and blocked HB-EGF shedding. The main signal transduction pathway leading to cardiac hypertrophy seems likely to be mediated by ADAM12 shedding of HB-EGF in cardiomyocytes.

In our aortic-banding model, we showed that KB-R7785 not only attenuated cardiac hypertrophy resulting from pressure overload, but also improved cardiac function. These results confirm recent reports suggesting the effectiveness of MMP inhibitors for heart failure[15]. Because it is unclear that the cardiac hypertrophy in the aortic-banding model is directly mediated through GPCRs, we further tested whether KB-R7785 attenuates cardiac hypertrophy induced by either PE or Ang II infusion. The results indicate that the metalloproteinase inhibitor blocks cardiac hypertrophy directly mediated through GPCRs. Together, our observations indicate that certain metalloproteinase inhibitors may be clinically effective for delaying the progression of heart failure following cardiac hypertrophy, or even for treating cardiac impairment that develops before the uncompensated phase of cardiac hypertrophy.

Thus, we conclude that cellular signaling in cardiomyocytes following treatment with GPCR agonists is dependent upon EGFR transactivation triggered by ADAM12-mediated cleavage of HB-EGF. This is the first demonstration that inhibition of HB-EGF shedding can lessen cardiac hypertrophy both *in vivo* and *in vitro*, and suggests that both HB-EGF and ADAM12 are potential targets for the treatment of cardiac hypertrophy.

Methods

Materials. PE, Ang II and ET-1 were purchased from Sigma. A mouse monoclonal anti-phosphotyrosine antibody 4G10, and a sheep polyclonal antibody to EGFR were from Upstate Biotechnology (Lake Placid, New York). A goat polyclonal antibody against EGFR was from Santa Cruz Biotechnology (Santa Cruz, California). The HB-EGF neutralizing polyclonal antibody #19 was from J.A. Abraham. KB-R7785 ([4-(*N*-hydroxyamino)-2R-isobutyl-3S-methylsuccinyl]-L-phenylglycine-*N*-methylamide), OSU7-6 and OSU9-6 were synthesized by Organon Japan (Osaka, Japan). Adenovirus carrying genes encoding LacZ, WT-ADAM12 and ΔMP-ADAM12 were prepared using adenovirus expression vector kit (Takara Biomedicals, Tokyo, Japan).

Cell culture. Primary cultures of neonatal rat cardiomyocytes were prepared as described[3]. Cells from hearts of 1–2-day-old Wistar rats were seeded onto 60-mm collagen-coated dishes (2×10^6 cells per dish) or 96-well plates in MEM medium supplemented with 10% FCS. After incubation for 18 h, the medium was replaced with MEM plus insulin, transferrin and sodium selenite 24 h before experiments.

EGFR immunoprecipitation in cardiomyocytes. Cultured cardiomyocytes were exposed to the agents (1×10^{-8} M HB-EGF, 1×10^{-5} M PE, 10^{-8} M Ang II, and 1×10^{-7}M ET-1) for 5 min except in Fig. 1 after pretreatment for 30 min with or without reagents (1 μM of KB-R7785 and 10 μg/ml of HB-EGF neutralizing antibody). Cells were lysed by incubation for 20 min at 4 °C in a buffer (50 mM Tris-HCl, pH 7.3; 150 mM NaCl; 2 mM EDTA; 0.5% sodium fluoride; 10 mM sodium pyrophosphate; 0.5 mM Na_3VO_4, 100 μg/ml phenylmethylsulfonyl fluoride; 2 μg/ml aprotinin; protease inhibitor cocktail; and 1 % Nonidet P-40). Immunoblotting analyses using 4G10 or antibody against EGFR were as described[16]. Cultured cardiomyocytes infected with adenovirus vectors (at multiplicity of infection 50) for 24 h were also subjected to EGFR immunoprecipitation analysis.

Incorporation of [^{3}H]leucine. Protein synthesis in cardiomyocytes was evaluated by incorporation of [^{3}H]leucine into cells. Following serum withdrawal, myocytes were exposed to compounds in MEM medium for 18 h, incubated with 1 μCi/ml [^{3}H]leucine for 12 h and washed once with PBS. The cells were attached to glass filter mats by a microharvester. Radioactivity was measured by a liquid scintillation counter (Wallac β-plate, Finland).

Yeast two-hybrid screening and assay. A human heart cDNA library (Clontech Japan, Tokyo, Japan) were used for large-scaled transformation of yeast cells (CG1945) carrying the pPKC-δ RD bait plasmid (gift from Y. Ono). The interacting cDNA clones were selected by growth on plates lacking histidine. Histidine-positive colonies were screened for LacZ expression by a colony lift method according to the manufacturer's instructions.

HB-EGF-AP shedding assay. Plasmids, pcDNA3.1 (Invitrogen, Carlsbad, California), human WT-ADAM12-flag/pcDNA3.1 and human ΔMP-ADAM12-flag/pcDNA3.1 were introduced into HT1080/HB-AP cells using lipofectamine (Gibco BRL, Rockville, Maryland). Stable transfectants were seeded in 24-well plates (1×10^5 cells per well) and then incubated for 24 h. The cells were incubated for an indicated time at 37 °C with 1×10^{-5} M PE. 50-μl aliquots of the conditioned media were transferred to 96-well plates, and AP activity was measured as described[16].

Transverse aortic banding. Pressure-overload cardiac hypertrophy was induced by transverse aortic banding in 8-wk-old male C57BL/6J mice (20–25 g). Suture was tied twice around a 27-gauge needle, which was positioned adjacent to the aorta between the right and left carotid arteries, and was removed after placement of the ligature. This yielded an outer diameter of approximately 0.3 mm (60–80% constriction). Mice were treated i.p. with or without KB-R7785 (100 mg/kg/d) for 4 wk.

Pharmacological induction of hypertrophy. 8-wk-old C57BL/6J male mice or 7-wk-old FVB male mice were treated with PE (30 mg/kg/day), Ang II (200 ng/kg/min) or vehicle by osmotic minipump (Alzet, California) to induce cardiac hypertrophy as reported[20,21]. In the KB-R7785 treatment group, KB-R7785 was administered daily (i.p.) during PE or Ang II treatment. After systemic blood pressure and heart rate were measured (BP-98A, Softron, Tokyo), mice with PE treatment were killed at 7 d after implantation of pumps and mice with Ang II treatment were killed at 14 d.

Echocardiography. Mice were anesthetized by pentobarbital (50 mg/kg) and the extent of cardiac hypertrophy was assessed by 15-MHz pulsed-wave Doppler echocardiography (Philips, SONOS5500, the Netherlands). We measured posterior-wall thickness (PWT), systolic left-ventricular diameter (LVDs), diastolic left-ventricular diameter (LVDd) and fractional shortening (FS).

HB-EGF immunoblotting. Mouse hearts were homogenized in 20 mM Tris-HCl (pH 7.2), 1.5 M NaCl, 1% Triton X-100, 1 mM EDTA (β-amidinophenyl) methanesulfonyl fluoride and 20 μg/ml aprotinin. After centrifugation at 15,000*g* for 10 min at 4 °C, supernatant aliquots (10 μg protein/aliquot) were fractionated by SDS-PAGE and immunoblotted using the polyclonal HB-EGF antibody #2998. HB-EGF was detected by alkaline phosphatase-conjugated secondary antibody.

Data analysis. Numerical data are reported as mean ± s.e.m. Data were analyzed statistically by Student's *t*-test.

Acknowledgments

We thank J.A. Abraham for helpful comments and advice; and J. Yamada, A. Ohno, T. Fukushima, A. Ogai and S. Mori for technical assistance. This study is supported by Grant-in-aid for Scientific Research (No. 09281102, 12370153 and 12877107) from the Ministry of Education, Science and Culture, Japan.

RECEIVED 28 JULY; ACCEPTED 5 NOVEMBER 2001

1. Katz, A.M. Cardiomyopathy of overload. A major determinant of prognosis in congestive heart failure. *N. Engl. J. Med.* **322**, 100–110 (1990).
2. Levy, D., Garrison, R.J., Savage, D.D., Kannel, W.B. & Castelli, W.P. Prognostic implications of echocardiographically determined left ventricular mass in the Framingham Heart Study. *N. Engl. J. Med* **322**, 1561–1566 (1990).
3. Simpson, P., McGrath, A. & Savion, S. Myocyte hypertrophy in neonatal rat heart cultures and its regulation by serum and by catecholamines. *Circ. Res.* **51**, 787–801 (1982).
4. Ito, H. *et al.* Endothelin-1 induces hypertrophy with enhanced expression of muscle-specific genes in cultured neonatal rat cardiomyocytes. *Circ. Res.* **69**, 209–215 (1991).
5. Sadoshima, J., Xu, Y., Slayter, H.S. & Izumo, S. Autocrine release of angiotensin II mediates stretch-induced hypertrophy of cardiac myocytes in vitro. *Cell* **75**, 977–984 (1993).
6. Schmieder, R.E., Martus, P. & Klingbeil, A. Reversal of left ventricular hypertrophy in essential hypertension. A meta-analysis of randomized double-blind studies. *JAMA* **275**, 1507–1513 (1996).
7. Effects of enalapril on mortality in severe congestive heart failure. Results of the Cooperative North Scandinavian Enalapril Survival Study (CONSENSUS). The CONSENSUS Trial Study Group. *N. Engl. J. Med.* **316**, 1429–1435 (1987).
8. Chien, K.R. *et al.* Transcriptional regulation during cardiac growth and development. *Annu. Rev. Physiol.* **55**, 77–95 (1993).
9. Sadoshima, J. & Izumo, S. The cellular and molecular response of cardiac myocytes to mechanical stress. *Annu. Rev. Physiol.* **59**, 551–571 (1997).
10. Daub, H., Weiss, F.U., Wallasch, C. & Ullrich, A. Role of transactivation of the EGF receptor in signalling by G-protein-coupled receptors. *Nature* **379**, 557–560 (1996).
11. Tsai, W., Morielli, A.D. & Peralta, E.G. The m1 muscarinic acetylcholine receptor transactivates the EGF receptor to modulate ion channel activity. *EMBO J.* **16**, 4597–4605 (1997).
12. Zwick, E. *et al.* Critical role of calcium-dependent epidermal growth factor receptor transactivation in PC12 cell membrane depolarization and bradykinin signaling. *J. Biol. Chem.* **272**, 24767–24770 (1997).
13. Eguchi, S. *et al.* Calcium-dependent epidermal growth factor receptor transactivation mediates the angiotensin II-induced mitogen-activated protein kinase activation in vascular smooth muscle cells. *J. Biol. Chem.* **273**, 8890–8896 (1998).
14. Prenzel, N. *et al.* EGF receptor transactivation by G-protein-coupled receptors requires metalloproteinase cleavage of proHB-EGF. *Nature* **402**, 884–888 (1999).
15. Spinale, F.G. *et al.* Matrix metalloproteinase inhibition during the development of congestive heart failure: effects on left ventricular dimensions and function. *Circ. Res.* **85**, 364–376 (1999).
16. Tokumaru, S. *et al.* Ectodomain shedding of epidermal growth factor receptor ligands is required for keratinocyte migration in cutaneous wound healing. *J. Cell Biol.* **151**, 209–220 (2000)
17. Goishi, K.*et al.* Phorbol ester induces the rapid processing of cell surface heparin-binding EGF-like growth factor: Conversion from juxtacrine to paracrine growth factor activity. *Mol. Biol. Cell* **6**, 967–980 (1995).
18. Izumi, Y. *et al.* A metalloprotease-disintegrin, MDC9/meltrin-γ/ADAM9 and PKCδ are involved in TPA-induced ectodomain shedding of membrane-anchored heparin-binding EGF-like growth factor. *EMBO J.* **17**, 7260–7272 (1998).
19. Moss, M.L. *et al.* Cloning of a disintegrin metalloproteinase that processes precursor tumour-necrosis factor-α. Nature **385**, 733–736 (1997).
20. Friddle, C.J., Koga, T., Rubin, E.M. & Bristow, J. Expression profiling reveals distinct sets of genes altered during induction and regression of cardiac hypertrophy. *Proc. Natl. Acad. Sci. USA* **97**, 6745–6750 (2000).
21. Saadane, N., Alpert, L. & Chalifour, L.E. Expression of immediate early genes, GATA-4, and Nkx-2.5 in adrenergic-induced cardiac hypertrophy and during regression in adult mice. *Br. J. Pharmacol.* **127**, 1165–1176 (1999).
22. Higashiyama, S., Lau, K., Besner, G., Abraham, J. A. & Klagsbrun, M. Structure of heparin-binding EGF-like growth factor: Multiple forms, primary structure, and glycosylation of the mature protein. *J. Biol. Chem.* **267**, 6205–6212 (1992).

THE JOURNAL OF BIOLOGICAL CHEMISTRY
Vol. 277, No. 46, Issue of November 15, pp. 43707–43716, 2002
Printed in U.S.A.

Specific Molecular Interactions of Oversulfated Chondroitin Sulfate E with Various Heparin-binding Growth Factors

IMPLICATIONS AS A PHYSIOLOGICAL BINDING PARTNER IN THE BRAIN AND OTHER TISSUES*

Received for publication, July 16, 2002, and in revised form, September 3, 2002
Published, JBC Papers in Press, September 6, 2002, DOI 10.1074/jbc.M207105200

Sarama Sathyaseelan Deepa‡§, Yuko Umehara‡§, Shigeki Higashiyama¶, Nobuyuki Itoh‖, and Kazuyuki Sugahara‡**

From the ‡Department of Biochemistry, Kobe Pharmaceutical University, Higashinada-ku, Kobe 658-8558, the ¶Department of Medical Biochemistry, Ehime University School of Medicine, Shitsukawa, Shigenobu-cho, Onsen-gun, Ehime 791 0295, and the ‖ Department of Genetic Biochemistry, Kyoto University Graduate School of Pharmaceutical Sciences, Kyoto 606-8501, Japan

We previously observed that the cortical neuronal cell adhesion mediated by midkine (MK), a heparin (Hep)-binding growth factor, is specifically inhibited by oversulfated chondroitin sulfate-E (CS-E) (Ueoka, C., Kaneda, N., Okazaki, I., Nadanaka, S., Muramatsu, T., and Sugahara, K. (2000) *J. Biol. Chem.* 275, 37407–37413) and that CS-E exhibits neurite outgrowth promoting activities toward embryonic rat hippocampal neurons. We have also shown oversulfated CS chains in embryonic chick and rat brains and demonstrated that the CS disaccharide composition changes during brain development. In view of these findings, here we tested the possibility of CS-E interacting with Hep-binding growth factors during development, using squid cartilage CS-E. The binding ability of Hep-binding growth factors (MK, pleiotrophin (PTN), fibroblast growth factor-1 (FGF-1), FGF-2, Hep-binding epidermal growth factor-like growth factor (HB-EGF), FGF-10, FGF-16, and FGF-18) toward [^{3}H]CS-E was first tested by a filter binding assay, which demonstrated direct binding of all growth factors, except FGF-1, to CS-E. The bindings were characterized further in an Interaction Analysis system, where all of the growth factors, except FGF-1, gave concentration-dependent and specific bindings. The kinetic constants k_a, k_d, and K_d suggested that MK, PTN, FGF-16, FGF-18, and HB-EGF bound strongly to CS-E, in comparable degrees to the binding to Hep, whereas the intensity of binding of FGF-2 and FGF-10 toward CS-E was lower than that for Hep. These findings suggest the possibility of CS-E being a binding partner, a coreceptor, or a genuine receptor for various Hep-binding growth factors in the brain and possibly also in other tissues.

Proteoglycans (PGs)[1] that bear heparan sulfate (HS) glycosaminoglycan side chains have attracted much attention because of the demonstration of the involvement of HS in the developmental processes and specific signaling pathways (for review, see Refs. 1–3). Although the chondroitin sulfate (CS) glycosaminoglycan side chains of CS-PGs have attracted less attention until recently, accumulating evidence suggests the importance of these molecules in various biological functions (2, 4). CS-PGs are also ubiquitous components of the extracellular matrix of connective tissues and are also found at the surfaces of many cell types and in intracellular secretory granules (for review, see Refs. 5 and 6). Developmentally regulated expression of CS epitopes in the rodent fetus has been demonstrated by immunological studies (7), especially during central nervous system development (8–10). CS is a rich component in the extracellular matrix of the brain (11). Developmentally regulated expression and tissue-specific distribution of CS variants suggest that CS chains differing in the degree and profile of sulfation perform distinct functions during development (12).

Among variant forms of CS chains, oversulfated CS chains, such as CS-E and CS-D, are of special interest. The presence of E (GlcUAβ1–3GalNAc(4*S*,6*S*)) and D (GlcUA(2*S*)β1–3GalNAc(6*S*)) units in bovine brain (13) and E18 rat brain (14) has been reported (GlcUA stands for D-glucuronic acid whereas 2*S*, 4*S*, and 6*S* represent 2-*O*-, 4-*O*-, and 6-*O*-sulfate, respectively). These units are present in appreciable proportions in chick brains, and their expression is regulated developmentally (15). Faissner *et al.* (16) demonstrated that the neurite outgrowth-stimulating capacity of DSD-1-PG, derived from neonatal mouse brains, is strongly reduced by the monoclonal antibody 473HD, which recognizes a CS epitope, and the interaction is inhibited by shark cartilage CS-C. We have shown that CS-D, an oversulfated CS also derived from shark cartilage, inhibits the interactions between the monoclonal antibody 473HD and DSD-1-PG and also promotes neurite outgrowth of E18 hippocampal neurons (17, 18) and that the DSD-1-PG contains the D disaccharide unit, which is a rich and poor component in CS-D and CS-C, respectively. We have further observed that another oversulfated variant CS-E, derived from squid cartilage, also exhibits neurite outgrowth promoting activity, which is not inhibited by 473HD, suggesting a

* The work at Kobe Pharmaceutical University was supported in part by a science research promotion fund from the Japan Private School Promotion Foundation and Grant-in-aid for Scientific Research (B) 12557214. The costs of publication of this article were defrayed in part by the payment of page charges. This article must therefore be hereby marked "*advertisement*" in accordance with 18 U.S.C. Section 1734 solely to indicate this fact.

§ These authors contributed equally to this work.

** To whom correspondence should be addressed: Dept. of Biochemistry, Kobe Pharmaceutical University, 4-19-1 Motoyama-kita-machi, Higashinada-ku, Kobe 658-8558, Japan. (Tel.: Int +81–78-441–7570; Fax: Int +81–78-441–7569); E-mail: k-sugar@kobepharma-u.ac.jp.

[1] The abbreviations used are: PG(s), proteoglycan(s); BSA, bovine serum albumin; CS, chondroitin sulfate; E, embryonic day(s); EDAC, 1-ethyl-3-(3-dimethylaminopropyl)carbodiimide; ERK, extracellular signal-regulated kinase; FGF, fibroblast growth factor; HABA, 2-(4-hydroxyazobenzene) benzoic acid; HB-EGF, heparin-binding epidermal growth factor-like growth factor; Hep, heparin; HS, heparan sulfate; IAsys, Interaction analysis system; MES, 2-(*N*-morpholino)ethanesulfonic acid; MK, midkine; PBS, phosphate-buffered saline; PTN, pleiotrophin; PTP, protein-tyrosine phosphatase; R_{eq}, response at equilibrium; RPTP, receptor-like PTP; rh, recombinant human; rm, recombinant mouse; rr, recombinant rat; TBS, Tris-buffered saline.

different mechanism for CS-E-induced neurite outgrowth (17, 19).

Recently, we demonstrated that the neuronal cell adhesion, mediated by the heparin (Hep)-binding growth factor midkine (MK), was specifically inhibited not only by Hep but also by squid cartilage oversulfated CS-E (14), although it was not inhibited by bovine kidney HS or other CS isoforms. Maeda *et al.* (20) identified pleiotrophin (PTN), a Hep-binding growth-associated molecule, as a 6B4-PG/phosphacan-binding protein in postnatal day 16 rat brain, and this binding was inhibited by CS-C. 6B4-PG/phosphacan is a major PG in the brain and corresponds to the extracellular region of a receptor-like protein-tyrosine phosphatase, PTPζ/RPTPβ (20, 21) and recently turned out to be identical with DSD-1-PG (22). MK and PTN constitute a unique family of Hep-binding proteins and share 45% sequence homology at the amino acid level (23, 24) in addition to many neuroregulatory activities including promotion of neurite outgrowth (25–27). PTN binds to the CS moiety of not only phosphacan, but also neurocan, another major CS-PG, in the brain (28). The CS chain of PTPζ shows high affinity binding to MK, which is inhibited by CS-C, CS-D, and CS-E (29). Zou *et al.* (30) also showed that MK bound to oversulfated CS chains with a dermatan sulfate-like domain in PG-M/versican, another CS-PG expressed in midgestation mouse embryos. Despite a large number of CS-PGs identified in the mammalian brain, CS chains attached to individual core proteins have not been structurally characterized, and the specificity of the molecular interactions of the brain CS chains with these growth factors has been largely unknown. However, we found recently that appican, the PG form of amyloid precursor protein, which is a neurotrophic factor (31), contained a significant proportion (14.3%) of E unit (32), demonstrating for the first time the presence of E unit in a particular brain CS-PG.

In view of the findings that MK and PTN are expressed in the brain during embryonic development and the demonstration of oversulfated CS structures, with binding capacities to these Hep-binding growth factors in embryonic brains, we hypothesized that these oversulfated structures might also interact with other Hep-binding growth factors in the brain during embryonic development. This hypothesis was explored in the present study using oversulfated CS-E in particular and various Hep-binding growth factors. The results suggest that all of the tested growth factors can indeed bind CS-E, and kinetic studies show that some of these bindings are stronger than those toward Hep. The preliminary findings have been reported in abstract form (33).

EXPERIMENTAL PROCEDURES

Materials—Recombinant human (rh)-MK expressed in *Escherichia coli* and rh-fibroblast growth factor-1, (FGF-1 or acidic FGF) expressed in *E. coli* was from PeproTech EC LTD (London, England). rh-PTN expressed in *E. coli* from RELIA *Tech* GmbH was from Braunschweig, Germany. rh-Hep-binding epidermal growth factor-like growth factor (HB-EGF) expressed in *Sf* 21 insect cells was from R&D systems (Minneapolis). rh-FGF-2 (basic FGF) expressed in *E. coli* was from Genzyme TECHNE (Minneapolis). rh-FGF-10 expressed in *E. coli* was provided by Takashi Katsumata (Sumitomo Pharmaceutical Research Center, Osaka, Japan). Recombinant rat (rr)-FGF-16 and recombinant mouse (rm)-FGF-18 were prepared as reported previously (34, 35). CS-E sodium salt (super special grade) from squid cartilage (average molecular mass of 70 kDa) (14) and bovine serum albumin (BSA) were purchased from Seikagaku Corp. (Tokyo, Japan), and porcine intestinal Hep sodium salt (200 IU/mg) (average molecular mass of 15 kDa) (14) was purchased from Nacalai Tesque, Inc. (Kyoto, Japan). EZ-Link® biotin-LC-hydrazide, ImmunoPure® avidin, and ImmunoPure® HABA were purchased from Pierce. BD BioCoat® streptavidin assay plates (96-well clear, flat bottom) were purchased from BD Biosciences (Bedford, MA). Goat anti-human MK antibody (IgG type) was purchased from Genzyme-Techne (Minneapolis). Alkaline phosphatase-conjugated AffiniPure rabbit anti-goat IgG (H+L) was purchased from Jackson ImmunoResearch Laboratories, Inc. (West Grove, PA). *p*-Nitrophenyl phosphate hexahydrate (disodium salt) was purchased from Wako Pure Chemical Industries, Ltd. (Osaka, Japan). Phosphate-buffered saline (PBS) tablets were purchased from Dainippon Pharmaceutical Co. Ltd. (Osaka, Japan). [^{3}H]Acetyl-labeled CS-E (1.463×10^6 cpm/μg) was prepared as described previously (36) by *N*-deacetylation with hydrazine followed by *N*-reacetylation with [^{3}H]$(CH_3CO)_2O$. [^{3}H]Glucosamine-labeled Hep sodium salt (2.85×10^5 cpm/μg) was purchased from PerkinElmer Life Sciences.

Filter Binding Assay—Filter binding assays for various growth factors with CS-E and Hep were performed as described previously (36) with slight modifications. Varying amounts (150–450 ng) of individual growth factors were incubated with [^{3}H]CS-E (82 ng, ~12,000 cpm), or a fixed amount (300 ng) of individual growth factors was incubated with [^{3}H]Hep (80 ng, ~22,800 cpm) in 50 μl of 50 mM Tris-HCl, pH 7.3, containing 130 mM NaCl and 1 mg/ml BSA at room temperature for 3 h. Mixed cellulose ester filters (0.45-μm or 1.0-μm pore size, 25-mm diameter; ADVANTEC, Tokyo) were placed onto a 12-well vacuum-assisted manifold filtration apparatus and washed with 10 ml of the same buffer devoid of BSA. The growth factor along with any bound [^{3}H]CS-E/Hep was recovered by the quick passage of the samples through the filters, and the unbound samples were eluted by washing five times with 2 ml of the same buffer. Protein-bound radioactivity was determined after immersing the filters in 1 ml of 1 M NaCl and 0.05 M diethylamine, pH 11.5, for 30 min and the radioactivity in the eluate was determined in a liquid scintillation counter (LSC-700, Aloka Co., Tokyo) using scintillation fluid containing 1.2% (w/v) 2,5-diphenyloxazole and 33% (w/v) Triton X-100.

Preparation of Biotinylated Hep and Biotinylated CS-E (37)—Hep or CS-E was dissolved in 100 mM MES, pH 5.5, at a concentration of 2 mg/ml. The solution was mixed with a 50 mM solution of freshly prepared biotin-LC-hydrazide (Pierce) in dimethyl sulfoxide. The weight ratio of Hep or CS-E to biotin-LC-hydrazide was 20:1. EDAC hydrochloride, dissolved in the same buffer, was added to this mixture. The weight ratio of Hep or CS-E to EDAC hydrochloride was 8:1. The labeling reaction occurred overnight at room temperature by gently mixing the solution. The reaction mixture was dialyzed against PBS at room temperature for 24 h. Dialysis was carried out in a Spectra/Por molecular porous membrane tubing, with a molecular mass cutoff of 3,500 Da (Spectrum Medical Industries, Inc., Laguna Hills, CA). Hexuronic acid in each preparation was quantified by the carbazole method, using GlcUA as standard (38). The mol of biotin/mol of CS-E or Hep was determined by the modified protocol of Green (39), which uses HABA dye and avidin, which form a complex. In brief, 60 μl of 10 mM HABA in 10 mM NaOH was added to 1.94 ml of 100 mM sodium phosphate, 150 mM NaCl, pH 7.2, containing 1 mg of avidin. The absorbance of this solution at 500 nm was recorded. A solution (10 μl each) of biotinylated CS-E (1.7 mg/ml) or Hep (2.1 mg/ml) was added to 90 μl of the above reagent. A decrease in absorbance, as biotin replaced HABA, was recorded. About 4.2% of the hexuronic acid groups in CS-E were derivatized with the biotin tag. The extent of biotinylation for Hep cannot be determined because addition of Hep produced a precipitate (40). However, a comparable degree of biotinylation with CS-E is expected for Hep.

Successful biotinylation of Hep or CS-E was confirmed by enzyme-linked immunosorbent assay. In brief, 2 μg of biotinylated Hep or CS-E was immobilized on a 96-well BD BioCoat® streptavidin assay plate. After overnight blocking with 3% BSA in PBS, 1 pmol of MK in PBS was added to each well followed by incubation at room temperature for 1 h. Goat anti-human MK antibody (diluted 200-fold with PBS) was added to each well after washing with PBS containing 0.05% Tween 20 (PBST), followed by incubation for 2 h at room temperature. The wells were washed with Tris-buffered saline (TBS) containing 0.05% Tween 20 (TBST), and alkaline phosphatase-conjugated AffiniPure rabbit anti-goat IgG (diluted 5,000-fold in TBS) was added to each well and left for 1 h at room temperature. After TBST washing, *p*-nitrophenyl phosphate in bicarbonate buffer (0.1 M Na_2CO_3/$NaHCO_3$ containing 1 mM $MgCl_2$, pH 9.8) was added to the wells and the development of color was measured after 15 min, at 415 nm in a microplate reader (Bio-Rad model 550).

Immobilization of CS-E and Hep to the Interaction Analysis System (IAsys; Affinity Sensors, Cambridge, UK) Cuvette—Biotinylated CS-E and biotinylated Hep were immobilized individually on the surface of a biotin cuvette as follows. The sensor surface of a biotin cuvette (Affinity sensors, Cambridge, UK) was equilibrated with PBST. Streptavidin (2 μg) was immobilized on the biotin cuvette for 15 min, and 10 μg of biotinylated CS-E or biotinylated Hep was added to the cuvette after washing with PBST. Biotinylated CS-E gave a response of 42 arc

seconds corresponding to 0.3 ng of the sample, whereas biotinylated Hep gave a response of 39 arc seconds corresponding to 0.26 ng of the sample, indicating that ~0.003% of the biotinylated sample was immobilized (600 arc seconds correspond to 1 ng of protein/mm^2 of the 4-mm^2 cuvette surface). After 10 min the cuvette was again washed with PBST and blocked with 20 μg of BSA. The successful immobilization was tested by applying 200 ng of MK to the cuvette surface. It gave a response of 80 arc seconds for the CS-E cuvette and 125 arc seconds for the Hep cuvette. A control cuvette was prepared in a manner similar to that for the CS-E or Hep cuvette, except that no biotinylated sample was added for immobilization.

Binding Assays of Hep-binding Growth Factors to CS-E/Hep in the IAsys—A single binding assay consisted of the following steps. To the CS-E- or Hep-immobilized cuvette, which was preequilibrated with PBST, a known concentration of each growth factor (final volume 200 μl) was added to initiate the association phase, and the binding reaction was continued for 10 min. The cuvette was then washed three times with 200 μl of PBST, and the dissociation of the bound ligate into the bulk PBST was followed for 3 min. To remove the residual bound ligate and thus regenerate the immobilized ligand, the cuvette was washed with 200 μl of 1 M NaCl. The stirrer speed was maintained at 80% (a percentage value specifying the amplitude of stirrer oscillation at 140 Hz. The scale was linear with 0 corresponding to no oscillation and 100 corresponding to the maximum level), and the temperature was maintained at 25 °C throughout the experiment. The distribution of the immobilized CS-E or Hep and of the bound growth factor on the surface of the biosensor cuvette was inspected by examination of the resonance scan, which showed that at all times these molecules were distributed on the sensor surface and therefore were not microaggregated.

To determine the binding kinetics, growth factors at varying concentrations were applied to the cuvette in the running buffer, followed by dissociation and regeneration, as described previously. Binding parameters were calculated from the association and dissociation phases of the binding reactions using the FASTfit software (Affinity Sensors). Using FASTfit, a plot of the on-rate constant, k_{on} (obtained from association analysis) *versus* the ligand concentration was obtained. The slope of the line is the association rate constant, k_a, and the intercept value on the *y* axis is the dissociation rate constant, k_d. The equilibrium dissociation constant, K_d, was calculated from the ratio (k_d/k_a) of the dissociation and association rate constants.

For determination of K_d using the Scatchard plot analysis, the response at equilibrium, R_{eq}, was plotted against $R_{eq}/[L]$, where L was the ligate concentration. The slope of this plot equals $-1/K_a$, the association equilibrium constant, and K_d was calculated using the equation $K_d = 1/K_a$. For determination of K_d using the binding curve analysis, the ligate concentration [L] was plotted against R_{eq}, and the K_d was equal to the ligate concentration at $R_{max}/2$.

RESULTS

In view of our previous findings that the neuronal cell adhesion mediated by MK is specifically inhibited by oversulfated CS-E from squid cartilage (14) and the presence of the CS-disaccharide E and D units in bovine, rat, and chick brains (13–15), we explored the possibility of high affinity binding of various other Hep-binding growth factors expressed in the brain during embryonic development. The representative growth factors of the MK family, EGF family, and FGF family were chosen, and the interactions of CS-E with MK, PTN, HB-EGF, FGF-1, FGF-2, FGF-10, and FGF-18 were analyzed. In addition, FGF-16, which is not expressed in the brain but is expressed in the brown adipocytes of rat embryos (41), was also tested to clarify the generality of a binding capacity of a Hep-binding growth factor to CS-E. Even though FGF-16 and FGF-18 are believed to bind Hep, no report is available demonstrating the direct binding of these growth factors to Hep.

Demonstration of the Binding of CS-E to Hep-binding Growth Factors in an Aqueous Solution by Filter Binding Assay—In the preliminary experiments, 82 ng of a [^{3}H]CS-E preparation was incubated with a fixed amount (300 ng) of various growth factors separately, and the binding ability was evaluated using the filter binding assay. The same amount of [^{3}H]Hep was treated with the individual growth factors in the same manner as positive controls. The results are summarized in Fig. 1. The findings demonstrated direct binding of CS-E to

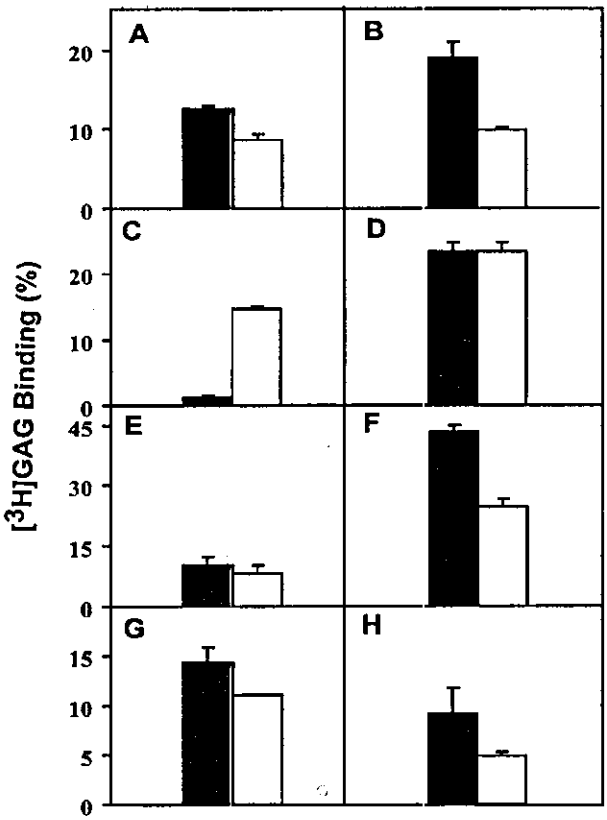

FIG. 1. **Binding of squid cartilage [^{3}H]CS-E to Hep-binding growth factors in an aqueous solution.** Squid cartilage [^{3}H]CS-E (82 ng, ~1.2 × 10^4 cpm) or [^{3}H]Hep (80 ng, 2.3 × 10^4 cpm) was incubated with 300 ng each of rh-MK (*A*), rh-PTN (*B*), rh-FGF-1 (*C*), rh-FGF-2 (*D*), rh-FGF-10 (*E*), rm-FGF-18 (*F*), rh-HB-EGF (*G*), and rr-FGF-16 (*H*). The radioactivity bound to each growth factor was quantified by the filter binding assay as described under "Experimental Procedures." Values were obtained from the average of two separate experiments and are expressed as percentages of the radioactivity added for incubation. Estimated errors were within 5%. *Filled bars* represent [^{3}H]CS-E, and *open bars* represent [^{3}H]Hep. *GAG*, glycosaminoglycan.

MK, PTN, HB-EGF, FGF-2, FGF-10, FGF-16, and FGF-18, whereas the binding of FGF-1 to CS-E was very low compared with those of other growth factors (Fig. 1*C*). The binding efficiency toward CS-E of all growth factors tested, except for FGF-1, was higher than that toward Hep, whereas FGF-2 exhibited the same degree of binding to CS-E and Hep. The degree of binding exhibited by most of the growth factors toward CS-E was in the range of 10–25%, except for FGF-1 (1.2%), whereas FGF-18 showed an exceptionally high degree of binding (~40%) (Fig. 1*F*). In the absence of any growth factor, the amount of CS-E or Hep bound to the filter was less than 0.2%.

To confirm the specificity of these bindings toward CS-E, the binding of varying concentrations of the growth factors (150, 300, and 450 ng) to a fixed concentration of CS-E (82 ng) was investigated by filter binding assay. All of the growth factors bound to CS-E in a dose-dependent manner. Even though FGF-1 also bound to CS-E in a dose-dependent manner, the extent of binding was far less compared with that of other growth factors (2% for FGF-1 compared with 15–50% for other growth factors). In the case of PTN, the saturation level was attained with 300 ng of the protein. However, saturation levels were not reached for all others even with 450 ng of the corresponding protein (data not shown), presumably because multi-

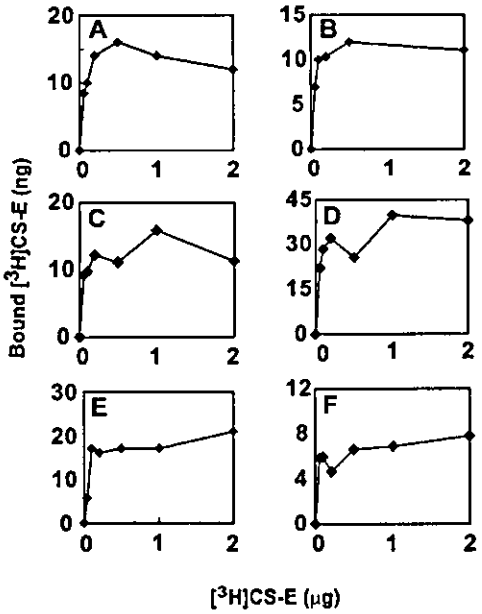

FIG. 2. **Saturation curves for the binding of squid cartilage [^{3}H]CS-E to Hep-binding growth factors in an aqueous solution.** Varying concentrations of squid cartilage [^{3}H]CS-E (0.05, 0.1, 0.2, 0.5, 1.0, and 2.0 μg) were incubated with 200 ng each of the Hep-binding growth factors, and the radioactivity bound to each growth factor was quantified by the filter binding assay as described under "Experimental Procedures." An equal amount of [^{3}H]CS-E without a growth factor was used as the negative control. Values were obtained by subtracting the radioactivity of the negative control from that of each sample. *A*, rh-PTN; *B*, rh-FGF-2; *C*, rh-FGF-10; *D*, rm-FGF-18; *E*, rh-HB-EGF; *F*, rr-FGF-16.

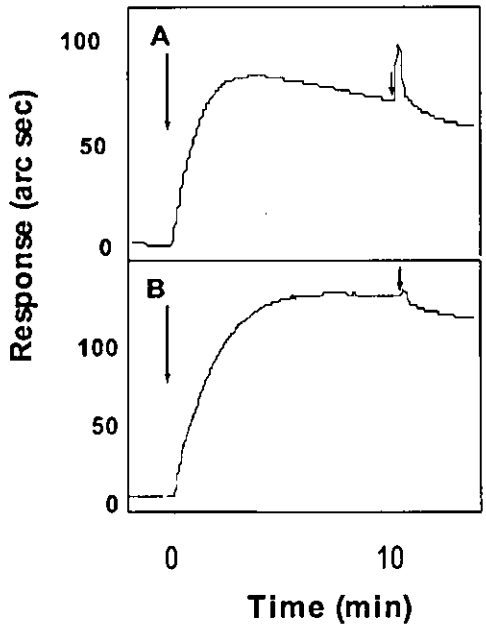

FIG. 3. **Sensorgrams for the binding of MK to CS-E- and Hep-immobilized cuvette.** Biotinylated CS-E or biotinylated Hep (10 μg) was immobilized on the streptavidin-coated surface of an IAsys cuvette, and 200 ng of MK was injected into CS-E-immobilized surface (*A*) and Hep-immobilized surface (*B*), individually, as described under "Experimental Procedures." *Long arrows* indicate the beginning of the association phase initiated by the injection of MK, and *short arrows* indicate the beginning of the dissociation phase initiated by washing with the running buffer.

ple binding sites for each growth factor are embedded along the CS-E chain. No higher concentrations were tested because of the limited availability of the proteins. As expected, [^{3}H]CS-E also exhibited a dose dependency for its binding toward these growth factors (Fig. 2). For a fixed amount (200 ng) of the individual growth factors, a saturation curve for [^{3}H]CS-E was observed with less than 1 μg each of all of the growth factors tested. FGF-1 also exhibited a similar trend, but only 1.2% of [^{3}H]CS-E was bound at the saturation level (data not shown). Together, these results suggest that the bindings of these growth factors, except for FGF-1, to CS-E were not caused merely by electrostatic interactions, but rather were highly specific.

Characterization of the Binding of the Various Hep-binding Growth Factors to Immobilized CS-E in the IAsys—The binding of growth factors to CS-E was characterized further using the IAsys, where CS-E was immobilized, and soluble growth factors were added as analytes to mimic physiological conditions. Biotinylated CS-E was immobilized onto the biotin-coated sensor surface of the IAsys cuvette via streptavidin as described under "Experimental Procedures." A Hep-immobilized cuvette was used to determine the positive control values. In both cases, 0.26~0.30 ng of the biotinylated sample was immobilized (see "Experimental Procedures"). The growth factors (200 ng each) were then added to the CS-E- or Hep-immobilized cuvette, individually, which had been equilibrated with PBST. Sensorgrams of the MK binding to the CS-E and Hep cuvettes are shown as representatives in Fig. 3. The binding of the growth factor to immobilized CS-E or Hep was indicated by a steady increase in the response with time up to 10 min, representing the association phase. This was followed by a dissociation phase generated by washing with PBST, and then the sensor surface was regenerated by washing with a 1 M NaCl solution. MK gave a response of 80 arc seconds for the CS-E cuvette (Fig. 3*A*) and 125 arc seconds for the Hep cuvette (Fig. 3*B*), indicating that 0.5 ng and 0.8 ng of MK bound to the CS-E cuvette and Hep cuvette, respectively. The response factors generated by each growth factor differed from one another, when compared using a fixed concentration (200 ng) of an analyte, where all of the growth factors gave a higher response with the Hep cuvette than the CS-E cuvette (Fig. 4), except for FGF-18, which gave comparable responses for CS-E and Hep cuvettes (Fig. 4*F*). Even though FGF-1 bound to the CS-E cuvette appreciably (Fig. 4*C*), the degree of the binding was very low compared with that of other growth factors, consistent with the results of filter binding assays, where FGF-1 showed a lesser degree of binding to [^{3}H]CS-E (Fig. 1*C*). The binding of all growth factors to CS-A-, CS-C-, and CS-D-immobilized cuvettes was very low, comparable with their binding to the control cuvette without immobilized CS-E or Hep (data not shown), indicating that among the CS variants, CS-E exhibited high specificity for these growth factors like Hep. The filter binding assay using [^{3}H]CS-D also showed that its binding to MK was less than 2% compared with 12% obtained using [^{3}H]CS-E.

Kinetics of Growth Factor Binding to Immobilized CS-E—The kinetic parameters for the interaction of the growth factors with CS-E or Hep were determined by varying the concentrations of the individual growth factors and studying their interactions with CS-E- or Hep-immobilized cuvettes using the IAsys. Fig. 5, *A* and *C*, shows the overlay of sensorgrams obtained by applying varying concentrations of MK and PTN, respectively, to the CS-E-immobilized cuvette. Varying concentrations of MK or PTN were added to the CS-E-immobilized cuvette, which had been equilibrated with PBST. Fig. 5, *B* and *D*, shows the overlay of sensorgrams for varying concentrations

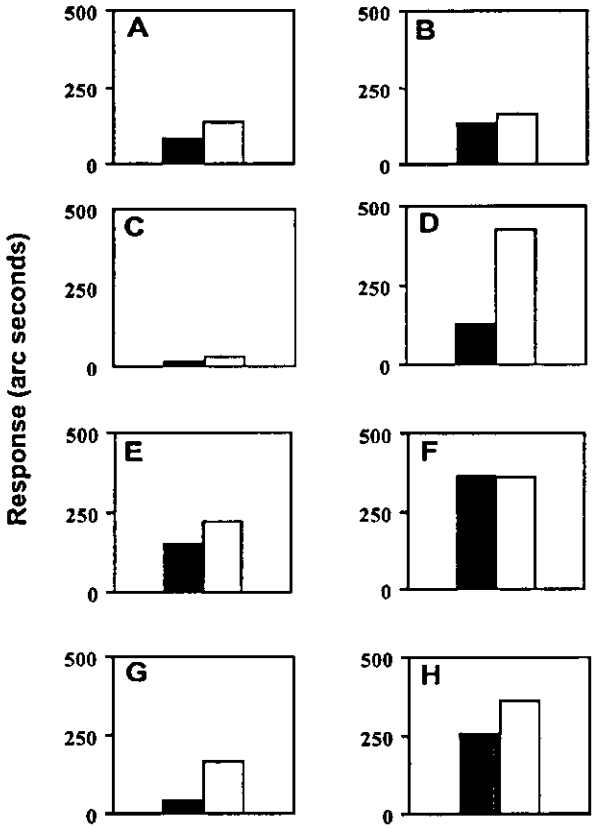

FIG. 4. **Analysis of the binding of Hep-binding growth factors to immobilized CS-E in an IAsys.** Biotinylated CS-E or biotinylated Hep (10 μg) was immobilized on the streptavidin-coated surface of an IAsys cuvette, and the Hep-binding growth factors (200 ng each) were injected individually into the CS-E-immobilized surface as described under "Experimental Procedures." Values on the *vertical axis* represent the change in resonance angle (response) expressed in arc seconds. Six hundred arc seconds correspond to 1 ng of protein/mm^2 of the cuvette surface. *A*, rh-MK; *B*, rh-PTN; *C*, rh-FGF-1; *D*, rh-FGF-2; *E*, rh-FGF-10; *F*, rm-FGF-18; *G*, rh-HB-EGF; *H*, rr-FGF-16. *Filled bars* represent CS-E, and *open bars* represent Hep.

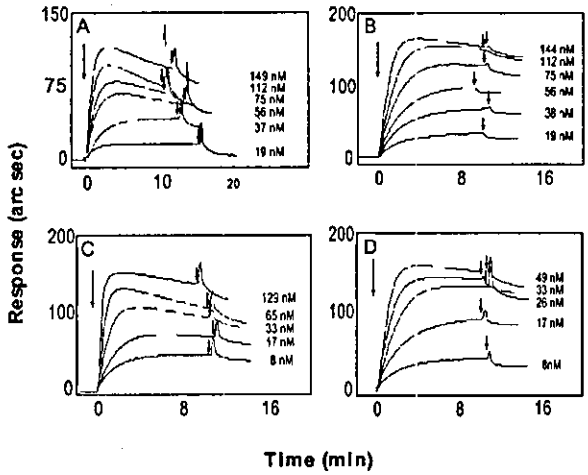

FIG. 5. **Overlaid sensorgrams for the CS-E binding and Hep binding kinetics of MK and PTN.** The binding assays were carried out as described in the legend to Fig. 4, except that the indicated concentrations of rh-MK (*A* and *B*) and rh-PTN (*C* and *D*) were applied to CS-E-immobilized (*A* and *C*) and Hep-immobilized (*B* and *D*) cuvettes. *Long arrows* indicate the beginning of the association phase initiated by the injection of varying concentrations of the growth factors, and *short arrows* indicate the beginning of the dissociation phase initiated by the running buffer.

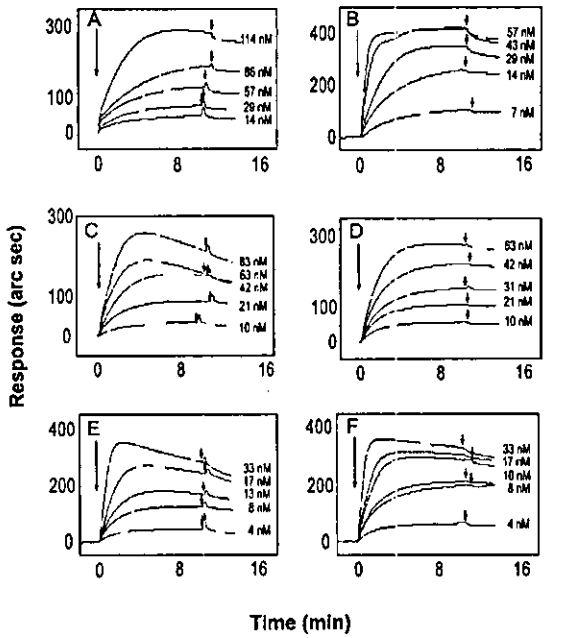

FIG. 6. **Overlaid sensorgrams for the CS-E binding and Hep binding kinetics of FGF-2, FGF-10, and FGF-18.** The binding assays were carried out as described in the legend to Fig. 4, except that the indicated concentrations of rh-FGF-2 (*A* and *B*), rh-FGF-10 (*C* and *D*), and rm-FGF-18 (*E* and *F*) were applied to CS-E-immobilized (*A*, *C*, and *E*) and Hep-immobilized (*B*, *D*, and *F*) cuvettes. *Long arrows* indicate the beginning of the association phase initiated by the injection of varying concentrations of the growth factors, and *short arrows* indicate the beginning of the dissociation phase initiated by the running buffer.

of MK and PTN toward Hep. At higher concentrations of analytes, a decrease in response, after reaching equilibrium in the association phase, was often observed for some sensorgrams, for example in Fig. 5*A*. This may be caused by either the physisorption, rather than chemisorption, of the growth factor to the sensor surface or the oligomerization of the growth factors at high concentrations. A sharp peak generated at the beginning of the dissociation phase in some of the sensorgrams was presumably caused by a shock by a sudden change in the refractive index or dielectric property created, when the cuvette was emptied and refilled with a fresh buffer. Both MK and PTN exhibited a dose-dependent binding toward CS-E and Hep. These growth factors gave a dose-dependent increase in response until it reached the saturation level. Their binding toward CS-E and Hep was monophasic, and there was no evidence for secondary binding sites.

The overlay of sensorgrams for FGF-2, FGF-10, and FGF-18, obtained by applying varying concentrations of these growth factors to the CS-E- and Hep-immobilized cuvette, is given in Fig. 6. The k_a, k_d, and K_d values for each growth factor were calculated using the FASTfit software, and the results are summarized in Table I. For each growth factor, only four sensorgrams of lower concentrations were used for calculating the parameters in most of the cases because excessive binding was observed at the highest concentration (for example, see Fig. 6, *C* and *E*) and may partially represent the physisorption or the oligomerization of growth factors as discussed above.

The k_a values for the binding of each growth factor to CS-E or Hep were different from one another. The k_a values for the binding of a given growth factor to CS-E and Hep were also

TABLE I

Kinetic parameters for the interaction of growth factors with immobilized CS-E and Hep

The apparent k_a, k_d, and K_d values for the interaction of Hep-binding growth factors with immobilized CS-E or Hep were determined using the IAsys as described under "Experimental Procedures." The S.E. is derived from the deviation of the data from a one-site binding model and was calculated by matrix inversion using the FASTfit software provided with the instrument. For each set of values of k_{on}, the resulting values for k_a and their associated S.E. were combined.

Growth factor	k_a	k_d	r^a	$K_d{}^b$
	$M^{-1}\ s^{-1}$	s^{-1}		nM
CS-E-immobilized cuvette				
MK	$1.1 \pm 0.3 \times 10^5$	$0.6 \pm 0.10 \times 10^{-2}$	0.938	61.6 ± 25.9
PTN	$4.5 \pm 0.4 \times 10^5$	$0.5 \pm 0.10 \times 10^{-2}$	0.992	11.4 ± 3.22
FGF-2	$3.3 \pm 0.3 \times 10^4$	$0.4 \pm 0.02 \times 10^{-2}$	0.987	119.8 ± 14.2
FGF-10	$6.5 \pm 2.0 \times 10^4$	$0.5 \pm 0.07 \times 10^{-2}$	0.918	88.6 ± 37.8
FGF-18	$5.7 \pm 2.3 \times 10^5$	$0.3 \pm 0.29 \times 10^{-2}$	0.930	8.9 ± 8.7
HB-EGF	$2.8 \pm 0.3 \times 10^6$	$4.2 \pm 0.30 \times 10^{-2}$	0.991	16.0 ± 18.4
Hep-immobilized cuvette				
MK	$3.5 \pm 1.5 \times 10^4$	$0.6 \pm 0.08 \times 10^{-2}$	0.853	204 ± 100
PTN	$2.6 \pm 0.9 \times 10^5$	$0.3 \pm 0.20 \times 10^{-2}$	0.902	16.1 ± 13.3
FGF-2	$2.4 \pm 0.2 \times 10^5$	$0.2 \pm 0.06 \times 10^{-2}$	0.991	8.6 ± 3.2
FGF-10	$1.4 \pm 0.3 \times 10^5$	$0.2 \pm 0.15 \times 10^{-2}$	0.966	17.4 ± 14.4
FGF-18	$6.3 \pm 2.9 \times 10^5$	$0.4 \pm 0.30 \times 10^{-2}$	0.833	10.8 ± 9.7
HB-EGF	$6.6 \pm 0.4 \times 10^5$	$0.3 \pm 0.10 \times 10^{-2}$	0.996	4.7 ± 3.67

[a] The correlation coefficient of the linear regression through the k_{on} values.

[b] The K_d value was calculated from the ratio k_d/k_a, and the S.E. is the combined S.E. of the two kinetic parameters.

different from each other. The k_a values for the binding of MK, PTN, and FGF-18 to the CS-E cuvette were approximately 1 order of magnitude larger than those for the binding of FGF-2 and FGF-10 to the CS-E cuvette. They were 1.1×10^5, 4.5×10^5, and $5.7 \times 10^5\ M^{-1}\ s^{-1}$, respectively, for the CS-E cuvette and 3.5×10^4, 2.6×10^5, and $6.3 \times 10^5\ M^{-1}\ s^{-1}$, respectively, for the Hep cuvette, suggesting that the binding rate of MK, PTN, and FGF-18 toward CS-E was higher or comparable with that toward Hep, under the conditions employed. In contrast, the k_a values of FGF-2 and FGF-10 for the CS-E cuvette were 3.3×10^4 and $6.5 \times 10^4\ M^{-1}\ s^{-1}$, respectively, and 2.4×10^5 and $1.4 \times 10^5\ M^{-1}\ s^{-1}$, respectively, for the Hep cuvette, suggesting a slower binding of these growth factors toward CS-E compared with the binding to Hep. The k_a values for FGF-2 and FGF-10 to Hep were ~7-fold and ~2-fold higher than those for the bindings to CS-E. On the other hand, the k_d values representing the dissociation rates of MK, PTN, FGF-2, FGF-10, and FGF-18 from the CS-E cuvette were comparable with those from the Hep cuvette. Consequently, the K_d values for the binding of MK, PTN, and FGF-18 with the CS-E cuvette were 61.6, 11.4, and 8.9 nM, respectively, and were lower or comparable with those for the Hep cuvette (204, 16.1, and 10.8 nM, respectively), whereas those for FGF-2 and FGF-10 for the CS-E cuvette were ~14-fold and ~5-fold higher, respectively, than those for the Hep cuvette. Thus, the difference in the K_d values appears to account for the differences in the k_a values.

The overlay of sensorgrams obtained by applying varying concentrations of HB-EGF, FGF-16, and FGF-1 to the CS-E- and Hep-immobilized cuvette is shown in Fig. 7. The sensorgram of HB-EGF for the CS-E cuvette (Fig. 7*A*) differed from the others. It showed an exceptionally sharp increase in response, reached a plateau within seconds of injecting the sample, and then showed a decrease in response with time (for low concentrations of the growth factor) even during the association phase. The dissociation phase of HB-EGF was also different from others in the fact that the dissociation rate was extremely high and reached a level close to the base line even before regeneration. The k_a values for the binding of HB-EGF to the CS-E and Hep cuvettes were 2.8×10^6 and 6.6×10^5, and the k_d values were 4.2×10^{-2} and 0.3×10^{-2}, respectively, for CS-E and Hep cuvettes. The k_a and k_d values of HB-EGF for the CS-E cuvette were 4-fold and 14-fold higher than those for the Hep cuvette. The K_d values for the binding of HB-EGF with the CS-E and Hep cuvette were 16 and 4.7 nM, respectively. Even though the K_d values for the CS-E and Hep cuvettes appear to be in the same range, the low K_d value for the CS-E cuvette was a result of the exceptionally high k_a and k_d values of HB-EGF toward the CS-E cuvette.

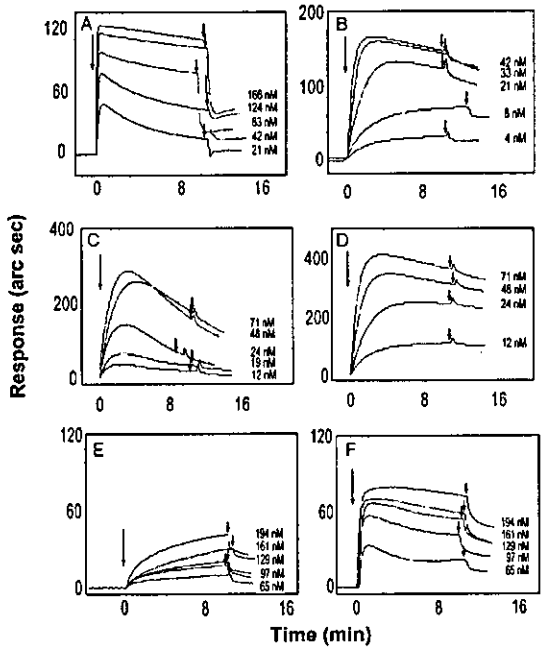

FIG. 7. **Overlaid sensorgrams for the CS-E binding and Hep binding kinetics of HB-EGF, FGF-16, and FGF-1.** The binding assays were carried out as described in the legend to Fig. 4, except that the indicated concentrations of rh-HB-EGF (*A* and *B*) rr-FGF-16 (*C* and *D*), and rh-FGF-1 (*E* and *F*) were applied to CS-E-immobilized (*A*, *C*, and *E*) and Hep-immobilized (*B*, *D*, and *F*) cuvettes, respectively. *Long arrows* indicate the beginning of the association phase initiated by the injection of varying concentrations of the growth factors, and *short arrows* indicate the beginning of the dissociation phase initiated by the running buffer.

The overlay of sensorgrams for FGF-16 for the CS-E cuvette (Fig. 7*C*) exhibited a peculiar pattern. Upon injection of the sample, there was a steady increase in response with time, and after reaching the plateau, a decline in response with time was observed during the association phase itself. As the concen-

TABLE II
Kinetic parameters for the interaction of FGF-16 and FGF-1 with immobilized CS-E and Hep

The K_d values for the interaction of FGF-16 for CS-E and Hep were calculated using Scatchard plot and binding curve analyses, and for FGF-1, the K_d value was calculated using Scatchard plot analysis, as described under "Experimental Procedures."

Growth factor	K_d			
	CS-E-immobilized cuvette		Hep-immobilized cuvette	
	Scatchard plot	Binding curve	Scatchard plot	Binding curve
	nM		*nM*	
FGF-16	47.2	70.0	34.7	44
FGF-1	1250.0	–[a]	149.3	–[a]

[a] A saturation level was not attained even with 2 μg of FGF-1 (see "Results").

tration of the growth factor was increased, this reduction in response became faster. The physiological significance of these binding patterns is not clear at this stage (and will be discussed later). The overlay of sensorgrams for FGF-1 for the CS-E cuvette (Fig. 7*E*) showed that the rate of its binding to CS-E is much slower compared with the quick rate of the binding to the Hep cuvette (Fig. 7*F*). Because the FASTfit software analysis failed to give a fit for FGF-16, K_d values were calculated using two other methods: Scatchard analysis and binding curve analysis, as described under "Experimental Procedures." The results are summarized in Table II. The K_d values obtained by the two different analyses were comparable, and the results showed that FGF-16 had almost comparable affinity for Hep and CS-E. This is the first report that demonstrates the direct binding of FGF-16 and FGF-18 to Hep. For FGF-1, a saturation level was not attained even with 2 μg of the growth factor, hence the binding curve analysis was not used for the determination of K_d value. The K_d value for FGF-1, obtained by Scatchard analysis (Table II), indicated that the affinity of FGF-1 to CS-E was very low and may explain the low degree of binding of FGF-1 to CS-E, although the K_d value for the Hep binding was comparable with the reported value (91 nM), which was determined by affinity coelectrophoresis (42).

From the IAsys experiments, it was possible to calculate average mol of each growth factor bound/mol of CS-E or Hep, taking the response of each growth factor at the saturation level. One mol of CS-E (70 kDa) or Hep (15 kDa) appears to have a capacity to bind a maximum of 13 or 4 mol of MK, 17 or 4 mol of PTN, 8 or 5 mol of HB-EGF, 14 or 9 mol of FGF-2, 11 or 5 mol of FGF-10, 17 or 7 mol of FGF-16, and 14 or 5 mol of FGF-18, respectively. These values indicate that a CS-E or Hep chain accommodates multiple yet different numbers of various growth factors, probably reflecting distinct yet overlapping growth factor binding sequences embedded in each sugar chain.

DISCUSSION

In the present study, we demonstrated the interaction of various Hep-binding growth factors with CS-E in two ways: the filter binding assay and analysis in the IAsys. In both situations, all of the tested growth factors, except for FGF-1, bound to CS-E in a dose-dependent manner, suggesting that these bindings are highly specific. Although these growth factors, except FGF-1, bound more strongly to CS-E than Hep in the filter binding assay, the reverse effects were observed in the IAsys, which may reflect the environment in which the two molecules are interacting. The IAsys more closely mimics the physiological conditions, where the soluble growth factors interact with CS chains in an immobilized form at the cell surface or in the extracellular matrices. On the other hand, complexes measured in the filter binding assay, where both interacting molecules are in solution, would mimic growth factor-CS complexes released enzymatically from cell surfaces or extracellular matrices.

MK and PTN specifically bound to CS-E derived from squid cartilage with high affinity (K_d = 61.6 and 11.4 nM, respectively), and these bindings were higher than or comparable with those for Hep (K_d = 204 and 16.1 nM, respectively), which is in reasonable agreement with our previous results obtained in a BiaCore system where the binding of soluble CS-E to immobilized MK was analyzed (14). The high affinity binding (K_d = 0.58 nM) of MK to PTPζ was reported, which was inhibited not only by CS-E but also by CS-B, CS-C, and CS-D (29). It was also reported that PG-M/versican isolated from E13 mouse embryos binds MK and PTN strongly (K_d = 1.0 nM), and the binding to MK is abolished by chondroitinase ABC digestion (30). The migration of osteoblast-like cells UMR 106 (43) and that of macrophages (44) promoted by MK are abolished by chondroitinases ABC or B digestion and also inhibited by exogenous CS-E in addition to CS-B. Maeda *et al.* (20) isolated PTN as a 6B4-PG/phosphacan-binding protein in the rat brain and also demonstrated that PTN binds to the CS moiety of phosphacan with high affinity (K_d = 0.25–3.0 nM), which was decreased by chondroitinase ABC digestion and was inhibited by CS-C. It was also reported that the PTN-stimulated migration of embryonic rat cortical neurons is inhibited by CS-C (21). However, in most studies, detailed structural information about the functional domain of the CS chains was lacking. In this context, our recent demonstration of the significant proportion of CS-E (14.3%) in the CS chain of appican PG (32) is highly significant and is the first demonstration of a specific brain CS-PG that contains the E unit. Previous studies have demonstrated that the CS chain in appican is responsible for the adhesion of neural cells and for promoting neurite outgrowth of primary rat hippocampal cultures, because the core of the Alzheimer's amyloid precursor protein is less potent in promoting adhesion and neurite outgrowth than appican PG (31, 46). The presence of E unit in appican PG may explain the neurotrophic activities of appican. Syndecan-1 from mouse mammary gland epithelial cells was also demonstrated to bear CS-E (48), although it is unknown whether syndecan-1 expressed in the rat central nervous system, which binds MK and PTN (49), contains CS-E.

CS-E also bound FGF family members. The FGF family comprises at least 23 proteins that play important roles in development, tissue maintenance, and tissue repair, and all family members have a Hep-binding property. The tested family members, except for FGF-16, are expressed in the brain. FGF-2 and FGF-10 bound to CS-E with lower affinity compared with Hep (based on K_d values). FGF-18 showed a strong binding, comparable with that toward Hep. In contrast, FGF-1 showed almost no binding. Each growth factor exhibited a peculiar association and dissociation pattern toward CS-E and Hep. The results appear to suggest that even lower affinity binding is physiologically significant as discussed below.

FGF-1 bound only weakly to CS-E, as indicated by a very high K_d value. The reason for this low affinity binding is unclear. Comparison of the Hep-binding domain of the tested FGF family members showed similar distribution of the basic amino acid residues. The only striking feature different from other FGF family members is the presence of the Cys^{137} residue within the Hep-binding domain (50). Structural characterization of the HS domain involved in the FGF-1 binding showed that the binding depends on a rarely occurring structure hall-

marked by L-iduronate(2-*O*-sulfate)-D-glucosamine(2-*N*-,6-*O*-disulfate) units (51). The human aorta HS preparation from an old individual, enriched in such units, showed drastically enhanced binding to FGF-1 (52) compared with HS from the young subject. The low degree of binding exhibited by FGF-1 to CS-E may be correlated with any of these observations.

FGF-2 binds N-syndecan, isolated from neonatal rat brain, with high affinity (K_d = 0.5 nM) through the HS chains, although FGF-1 fails to give such a binding toward N-syndecan (53). Based on the observation that N-syndecan mRNA levels in the neonatal rat brain are significantly higher than those in the adult rat brain, an important role of N-syndecan in nerve tissue differentiation has been suggested (54). Milev *et al.* (28) demonstrated that the core protein of phosphacan CS-PG showed high affinity binding toward FGF-2 and potentiated its mitogenic effect. Even if the binding of phosphacan to FGF-2 was reduced to 35% after chondroitinase treatment, the mitogenic effect generated by intact phosphacan was comparable with that exhibited by the core protein alone. This was the first demonstration that suggests that CS-PGs may also regulate the access of FGF-2 to cell surface signaling receptors in nervous tissues. The present finding that the FGF-2 interacts with CS-E suggests a possibility that E units in CS side chains of PGs, along with the core protein, may also be involved in the interaction with FGF-2, if it is expressed on certain CS-PGs at specific developmental stages.

Although FGF-10 mRNA is expressed predominantly in the lung, it is also expressed in the brain at low levels, being spatially restricted in some regions, including the hippocampus, thalamus, midbrain, and brainstem, and preferentially in neurons, but not in glial cells (55). Studies using FGF-10 knockout mice have demonstrated that this molecule is essential for limb and lung formation (56). Apart from this, the requirement of FGF-10 in the development of white adipose tissue (57) and its role as mitogen for urothelial cells (58) and in the maintenance of the stem cell compartment in developing mouse incisors (59) were reported recently. The possible involvement of CS-E in these biological events remains to be clarified.

FGF-18 is a unique secreted signaling molecule in the adult lung and developing tissues (60). However, the expression of FGF-18 in lower levels in the mouse brain has also been reported (35, 61). Ohuchi *et al.* (62) reported the involvement of FGF18-FGF8 signaling for specification of left-right symmetry and development of the chick embryo brain, especially the midbrain, and limbs. Novel roles for FGF-18 in calvarial and limb development (63) as well as in the proximal programming during lung morphogenesis have been reported (64). It is of particular interest to clarify whether E units in CS chains of certain CS-PGs are involved in the FGF-18 signaling in the above biological events, especially because FGF-18 binding to CS-E was exceptionally strong.

From the calculated K_d values, it appears that the affinity of FGF-16 toward CS-E is comparable with that for Hep. However, the pattern of the sensorgrams generated by FGF-16 with CS-E cuvette was markedly different from other growth factors in that they decreased significantly even during the association phase. Because this pattern closely resembles that generated by FGF-1 in a Hep-immobilized cuvette, there is a strong possibility that these bindings are physiologically significant. It will be interesting to clarify whether the binding of FGF-16 to CS-E can stimulate cellular growth or the signal transduction cascade *in vivo*. FGF-16 is expressed predominantly in the brown adipocytes of rat embryos during embryonic days 17.5–19.5 and appears to be a unique growth factor involved in the proliferation of embryonic brown adipose tissue (65). It also induces hepatocellular proliferation and increases liver weight *in vivo* (34). However, a truncated rat FGF-16 with 34 amino acids removed from the N terminus induces proliferation of oligodendrocytes, isolated from the rat brain, *in vitro* (34). It is noteworthy that FGF-16 shares 62% amino acid identity with FGF-20, whose mRNA is expressed preferentially in the brain among the adult rat major tissues and is reported to enhance the survival of midbrain dopaminergic neurons (66).

The high affinity of HB-EGF, an EGF family member (67, 68), toward CS-E observed in the present study, as indicated by the low K_d value, is interesting in that it is a consequence of the high association and dissociation rates (Table I). Thus, the kinetic studies have revealed the quick binding of the growth factor to CS-E in the environment of an increasing concentration of HB-EGF and its fast release with a decrease in the growth factor concentration. The polypeptides of EGF family produced by neurons and glial cells play important roles in the development of the nervous system, stimulating proliferation, migration, and differentiation of neuronal, glial, and Schwann precursor cells (69). Nakagawa *et al.* (70) reported the neuronal and glial expression of HB-EGF in the central nervous system of prenatal and early postnatal rats and suggested that it may contribute to brain development. HB-EGF is also reported to regulate the survival of midbrain dopaminergic neurons utilizing mitogen-activated protein kinase in addition to the Akt-signaling pathway (71). In addition, a new role of HB-EGF was reported recently by Asakura *et al.* (72), who found that the cleavage and shedding of the membrane-bound HB-EGF by metalloproteases contribute to the cardiac hypertrophic process and suggested that inhibition of HB-EGF shedding could be a potent therapeutic strategy for cardiac hypertrophy. It is of interest to clarify whether CS-PGs, in addition to HS-PGs, are involved in the regulation of these functions of HB-EGF. The physiological significance of the low affinity bindings caused by the slow binding observed for FGF-2 and FGF-10, compared with high affinity bindings, in addition to the quick binding and release of HB-EGF remains to be clarified. There is a possibility that these low affinity motifs act as a scaffold to capture the growth factors and then hand them over to other high affinity motifs and finally direct the growth factor toward the site of interaction with its receptor target at the cell surface (73). The graded affinities of various HS oligosaccharides for FGF-1 and FGF-2 (74, 75) are consistent with this concept. CS-E with higher affinity for certain growth factors than Hep may in turn receive them from HS chains as was discussed previously for a hybrid PG, syndecan-1 containing CS-E (48).

Although most studies of growth factor interactions with PGs have concerned HS-PGs and more specifically their HS-glycosaminoglycan chains, the present findings strengthen the emerging concept (4, 44) that the interactions of CS-PGs with growth/differentiation factors might also play significant roles in developmental processes of the central nervous system and other systems. In this context, Muramatsu (44) recently reported the isolation of CS that bound strongly to MK by affinity chromatography after labeling neurons from E13 embryos with [^{14}C]glucosamine. The disaccharide composition analysis of the strongly bound fraction showed that 30% was E unit. Kawashima *et al.* (76) recently demonstrated specific high affinity interactions of L- and P-selectins and chemokines with CS-E and suggested the involvement of the E unit-containing CS/dermatan sulfate in selectin- and/or chemokine-mediated cellular responses (76). The results obtained in the present study, together with accumulating evidence, may suggest the possibility that CS-glycosaminoglycan chains produced at certain

developmental stages act as a binding partner, a coreceptor, or a genuine receptor for various Hep-binding growth factors and chemokines/cytokines with developmentally regulated expression. Recently, Muramatsu (44) proposed a model of MK signaling through PTPζ, where the MK receptor is a molecular complex of PTPζ and a transmembrane protein, *viz.* low density lipoprotein receptor-related protein, which was reported to function as signaling receptors upon signal reception of Wnt and reelin. The essential function of PGs in this complex may be the activation of Src family kinases, by an as yet undetermined mechanism, which will in turn activate the phosphoinositide 3-kinase to ERK downstream signaling systems. It was also reported that the phosphoinositide 3-kinase to ERK pathway acts as a downstream signaling system for MK and PTN (77, 78).

Elucidation of the minimal structural units for these interactions will be essential for therapeutic strategies to develop drugs that may selectively interfere with CS-protein interactions. Development of CS-E-based drugs will certainly be a major breakthrough, because they can even substitute for endogenous CS in agonist mode. To achieve this, two major obstacles for such advancement have to be overcome: the lack of information regarding protein-binding epitopes in CS chains and the structural variability of CS molecules from different cells and tissues. The squid cartilage CS-E, used in the present study, has unusual GlcUA(3*S*)-containing disaccharide units such as GlcUA(3*S*)-GalNAc(4*S*), GlcUA(3*S*)-GalNAc(6*S*), and GlcUA(3*S*)-GalNAc(4*S*,6*S*), where 3*S* represents 3-*O*-sulfate (45, 47) in addition to the conventional E unit. Some of these heavily sulfated structures in CS-E are comparable with the highly sulfated regions in Hep. It is unclear whether these units are involved in the observed binding of the growth factors and whether such unique structures contribute to the binding of CS chains to these growth factors in mammalian systems because the existence of such structures in the mammalian system has not yet been reported.

REFERENCES

1. Sugahara, K., and Kitagawa, H. (2002) *IUBMB Life*, in press
2. Sugahara, K., and Kitagawa, H. (2000) *Curr. Opin. Struct. Biol.* **10**, 518–527
3. Perrimon, N., and Bernfield, M. (2000) *Nature* **404**, 725–728
4. Sugahara, K., and Yamada, S. (2000) *Trends Glycosci. Glycotechnol.* **12**, 321–349
5. Rodén, L. (1980) in *The Biochemistry of Glycoproteins and Proteoglycans* (Lennarz, W. J., ed) pp. 491–517, Plenum Publishing Corp., New York
6. Hascall, V. C., and Hascall, G. K. (1981) in *Cell Biology of Extracellular Matrix* (Hay, E. D., ed) pp. 39–63, Plenum Publishing Corp., New York
7. Mark, M. P., Baker, J. R., Kimata, K., and Ruch, J. V. (1990) *Int. J. Dev. Biol.* **34**, 191–204
8. Herndon, M. E., and Lander, A. D. (1990) *Neuron* **4**, 949–961
9. Lander, A. D. (1993) *Curr. Opin. Neurobiol.* **3**, 716–723
10. Ochira, A., Matsui, F., Tokita, Y., Yamauchi, S., and Aono, S. (2000) *Arch. Biochem. Biophys.* **374**, 24–34
11. Ruoslahti, E. (1989) *J. Biol. Chem.* **264**, 13369–13372
12. Poole, A. R. (1986) *Biochem. J.* **236**, 1–14
13. Saigo, K., and Egami, F. (1970) *J. Neurochem.* **17**, 633–647
14. Ueoka, C., Kaneda, N., Okazaki, I., Nadanaka, S., Muramatsu, T., and Sugahara, K. (2000) *J. Biol. Chem.* **275**, 37407–37413
15. Kitagawa, H., Tsutsumi, K., Tone, Y., and Sugahara, K. (1997) *J. Biol. Chem.* **272**, 31377–31381
16. Faissner, A., Clement, A., Lochter, A., Streit, A., Mandl, C., and Schachner, M. (1994) *J. Cell Biol.* **126**, 783–799
17. Nadanaka, S., Clement, A., Masayama, K., Faissner, A., and Sugahara, K. (1998) *J. Biol. Chem.* **273**, 3296–3307
18. Clement, A. M., Nadanaka, S., Masayama, K., Mandl, C., Sugahara, K., and Faissner, A. (1998) *J. Biol. Chem.* **273**, 28444–28453
19. Clement, A. M., Sugahara, K., and Faissner, A. (1999) *Neurosci. Lett.* **269**, 125–128
20. Maeda, N., Nishiwaki, T., Shintani, T., Hamanaka, H., and Noda, M. (1996) *J. Biol. Chem.* **271**, 21446–21452
21. Maeda, N., and Noda, M. (1998) *J. Cell Biol.* **142**, 203–216
22. Garwood, J., Schnadelbach, O., Clement, A., Schutte, K., Bach, A., and Faissner, A. (1999) *J. Neurosci.* **19**, 3888–3899
23. Kadomatsu, K., Tomomura, M., and Muramatsu, T. (1998) *Biochem. Biophys. Res. Commun.* **151**, 1312–1318
24. Merenmies, J., and Rauvala, H. (1990) *J. Biol. Chem.* **265**, 16721–16724
25. Rauvala, H. (1989) *EMBO J.* **8**, 2933–2941
26. Muramatsu, H., and Muramatsu, T. (1991) *Biochem. Cell Biol.* **177**, 652–658
27. Kaneda, N., Talukder, A. H., Nishiyama, H., Koizumi, S., and Muramatsu, T. (1996) *J. Biochem. (Tokyo)* **119**, 1150–1156
28. Milev, P., Monnerie, H., Popp, S., Margolis, R. K., and Margolis, R. U. (1998) *J. Biol. Chem.* **273**, 21439–21442
29. Maeda, N., Ichihara-Tanaka, K., Kimura, T., Kadomatsu, K., Muramatsu, T., and Noda, M. (1999) *J. Biol. Chem.* **274**, 12474–12479
30. Zou, K., Muramatsu, H., Ikematsu, S., Sakuma, S., Sulama, R. H., Shinomura, T., Kimata, K., and Muramatsu, T. (2000) *Eur. J. Biochem.* **267**, 4046–4053
31. Salinero, O., Moreno-Flores, M. T., and Wandosell, F. (2000) *J. Neurosci. Res.* **60**, 87–97
32. Tsuchida, K., Shioi, J., Yamada, S., Boghosian, G., Wu, A., Cai, H., Sugahara, K., and Robakis, N. K. (2001) *J. Biol. Chem.* **276**, 37155–37160
33. Deepa, S. S., Umehara, Y., Higashiyama, S., Itoh, N., and Sugahara, K. (2002) *23rd Japanese Carbohydrate Symposium*, Yokohama, Japan, August 22–24, 2002 (Hashimoto, H., ed) p. 91, Abstract PI-37, Gakushin Publishing Co., Suita, Japan
34. Danilenko, D. M., Montestruque, S., Philo, J. S., Li, T., Hill, D., Speakman, J., Bahru, M., Zhang, M., Konishi, M., Itoh, N., Chirica, M., Delaney, J., Hernday, N., Martin, F., Hara, S., Talvenheimo, J., Narhi, L. O., and Arakawa, T. (1999) *Arch. Biochem. Biophys.* **361**, 34–46
35. Hu, M. C., Qiu, W. R., Wang, Y. P., Hill, D., Ring, B. D., Scully, S., Bolon, B., DeRose, M., Luethy, R., Simonet, W. S., Arakawa, T., and Danilenko, D. M. (1998) *Mol. Cell. Biol.* **10**, 6063–6074
36. Yamane, Y., Tohno-oka, R., Yamada, S., Furuya, S., Shiokawa, K., Hirabayashi, Y., Sugino, H., and Sugahara, K. (1998) *J. Biol. Chem.* **273**, 7375–7378
37. Yang, B., Yang, B. L., and Goetinck, P. F. (1995) *Anal. Biochem.* **228**, 299–306
38. Bitter, M., and Muir, H. (1962) *Anal. Biochem.* **4**, 330–334
39. Green, N. M. (1965) *Biochem. J.* **94**, 23c–24c
40. Foxall, C., Holme, K. R., Liang, W., and Wei, Z. (1995) *Anal. Biochem.* **231**, 366–373
41. Miyake, A., Konishi, M., Martin, F. H., Hernday, N. A., Ozaki, K., Yamamoto, S., Mikami, T., Arakawa, T., and Itoh, N. (1998) *Biochem. Biophys. Res. Commun.* **243**, 148–152
42. Lee, M. K., and Lander, A. D. (1991) *Proc. Natl. Acad. Sci. U. S. A.* **88**, 2768–2772
43. Qi, M., Ikematsu, S., Maeda, N., Ichihara-Tanaka, K., Sakuma, S., Noda, M., Muramatsu, T., and Kadomatsu, K. (2001) *J. Biol. Chem.* **276**, 15868–15875
44. Muramatsu, T. (2001) *Trends Glycosci. Glycotechnol.* **13**, 563–572
45. Sugahara, K., Tanaka, Y., Yamada, S., Seno, N., Kitagawa, H., Haslam, S. M., Morris, H. R., and Dell, A. (1996) *J. Biol. Chem.* **271**, 26745–26754
46. Wu, A., Pangalos, M. N., Efthimiopoulos, S., Shioi, J., and Robakis, N. K. (1997) *J. Neurosci.* **17**, 4987–4993
47. Kinoshita, A., Yamada, S., Haslam, S. M., Morris, H. R., Dell, A., and Sugahara, K. (2001) *Biochemistry* **40**, 12654–12635
48. Ueno, M., Yamada, S., Zako, M., Bernfield, M., and Sugahara, K. (2001) *J. Biol. Chem.* **276**, 29134–29140
49. Nakanishi, T., Kadomatsu, K., Okamoto, T., Ichihara-Tanaka, K., Kojima, T., Saito, H., Tomoda, Y., and Muramatsu, T. (1997) *J. Biochem. (Tokyo)* **121**, 197–205
50. Patrie, K. M., Botelho, M. J., Franklin, K., and Chiu, I. M. (1999) *Biochemistry* **38**, 9264–9272
51. Kreuger, J., Prydz, K., Pettersson, R. F., Lindahl, U., and Salmivirta, M. (1999) *Glycobiology* **9**, 723–729
52. Feyzi E., Saldeen, T., Larsson, E., Lindahl, U., and Salmivirta, M. (1998) *J. Biol. Chem.* **273**, 13395–13398
53. Chernousov, M. A., and Carey, D. J. (1993) *J. Biol. Chem.* **268**, 16810–16814
54. Carey, D. J., Evans, D. M., Stahl, R. C., Asundi, V. K., Conner, K. J., Garbes, P., and Cizmeci-Smith, G. (1992) *J. Cell Biol.* **117**, 191–201
55. Hattori, Y., Yamasaki, M., Konishi, M., and Itoh, N. (1997) *Brain Res. Mol. Brain Res.* **47**, 139–146
56. Sekine, K., Ohuchi, H., Fujiwara, M., Yamasaki, M., Yoshizawa, T., Sato, T., Yagishita, N., Matsui, D., Koga, Y., Itoh, N., and Kato, S. (1999) *Nat. Genet.* **21**, 138–141
57. Sakaue, H., Kinoshi, M., Ogawa, W., Asaki, T., Mori, T., Yamasaki, M., Takata, M., Ueno, H., Kato, S., Kasuga, M., and Itoh, N. (2002) *Genes Dev.* **16**, 908–912
58. Bagai, S., Rubio, E., Cheng, J. F., Sweet, R., Thomas, R., Fuchs, E., Grady, R., Mitchell, M., and Bassuk, J. A. (2002) *J. Biol. Chem.* **277**, 23828–23837
59. Harada, S., Toyono, T., Toyoshima, K., Yamasaki, M., Itoh, N., Kato, S., Sekine, K., and Ohuchi, H. (2002) *Development* **129**, 1533–1541
60. Ohbayashi, N., Hoshikawa, M., Kimura, S., Yamasaki, M., Fukui, S., and Itoh, N. (1998) *J. Biol. Chem.* **273**, 18161–18164
61. Xu, J., Liu, Z., and Ornitz, D. M. (2000) *Development* **127**, 1833–1843
62. Ohuchi, H., Kimura, S., Watamoto, M., and Itoh, N. (2000) *Mech. Dev.* **95**, 55–66
63. Hajihosseini, M. K., and Heath, J. K. (2002) *Mech. Dev.* **113**, 79–83
64. Whitsett, J. A., Clark, J. C., Picard, L., Tichelaar, J. W., Wert, S. E., Itoh, N., Perl, A. K., and Stahlman, M. T. (2002) *J. Biol. Chem.* **277**, 22743–22749
65. Konishi, M., Mikami, T., Yamasaki, M., Miyake, A., and Itoh, N. (2000) *J. Biol. Chem.* **275**, 12119–12122
66. Ohmachi, S., Watanabe, Y., Mikami, T., Kusu, N., Ibi, T., Akaike, A., and Itoh, N. (2000) *Biochem. Biophys. Res. Commun.* **277**, 355–360
67. Higashiyama, S., Abraham, J. A., Miller, J., Fiddes, J. C., and Klagsbrun, M. (1991) *Science* **251**, 936–939
68. Higashiyama, S., Lau, K., Besner, G. E., Abraham, J. A., and Klagsbrun, M. (1992) *J. Biol. Chem.* **267**, 6205–6212
69. Xian, C. J., and Zhou, X. F. (1999) *Mol. Neurobiol.* **20**, 157–183
70. Nakagawa, T., Sasahara, M., Hayase, Y., Haneda, M., Yasuda, H., Kikkawa, R., Higashiyama, S., and Hazama, F. (1998) *Brain Res. Dev. Brain Res.* **108**, 263–272
71. Farkas, L. M., and Krieglstein, K. (2002) *J. Neural Transm.* **109**, 267–277
72. Asakura, M., Kitakaze, M., Takashima, S., Liao, Y. Ishikura, F., Yoshinaka,

T., Ohmoto, H., Node, K., Yoshino, K., Ishiguro, H., Asanuma, H., Sanada, S., Matsumura, Y., Takeda, H., Beppu, S., Tada, M., Hori, M., and Higashiyama, S. (2002) *Nat. Med.* **8,** 35–40
73. Lander, A. D. (1998) *Matrix Biol.* **17,** 465–472
74. Kreuger, J., Salmivirta, M., Sturiale, L., Gimenez-Gallego, G., and Lindahl, U. (2001) *J. Biol. Chem.* **276,** 30744–30752
75. Jemth, P., Kreuger, J., Kusche-Gullberg, M., Sturiale, L., Gimenez-Gallego, G., and Lindahl, U. (2002) *J. Biol. Chem.* **277,** 30567–30573
76. Kawashima, H., Atarashi, K., Hirose, M., Hirose, J., Yamada, S., Sugahara, K., and Miyasaka, M. (2002) *J. Biol. Chem.* **277,** 12921–12930
77. Owada, K., Sanjo, N., Kobayashi, T., Mizusawa, H., Muramatsu, H., Muramatsu, T., and Michikawa, M. (1999) *J. Neurochem.* **73,** 2084–2092
78. Souttou, B., Ahmad, S., Riegel, A. T., and Wellstein, A. (1997) *J. Biol. Chem.* **272,** 19588–19593

Molecular Biology of the Cell
Vol. 13, 2547–2557, July 2002

Ligand-independent Dimer Formation of Epidermal Growth Factor Receptor (EGFR) Is a Step Separable from Ligand-induced EGFR Signaling

Xiaochun Yu,† Kailash D. Sharma,† Tsuyoshi Takahashi,* Ryo Iwamoto,* and Eisuke Mekada*‡

*Department of Cell Biology, Research Institute for Microbial Diseases, Osaka University, Suita, Osaka 565-0871, Japan, and †Institute of Life Science, Kurume University, Kurume, Fukuoka 839-0861, Japan

Submitted August 16, 2001; Revised March 19, 2002; Accepted March 27, 2002
Monitoring Editor: Carl-Henrik Heldin

Dimerization and phosphorylation of the epidermal growth factor (EGF) receptor (EGFR) are the initial and essential events of EGF-induced signal transduction. However, the mechanism by which EGFR ligands induce dimerization and phosphorylation is not fully understood. Here, we demonstrate that EGFRs can form dimers on the cell surface independent of ligand binding. However, a chimeric receptor, comprising the extracellular and transmembrane domains of EGFR and the cytoplasmic domain of the erythropoietin receptor (EpoR), did not form a dimer in the absence of ligands, suggesting that the cytoplasmic domain of EGFR is important for predimer formation. Analysis of deletion mutants of EGFR showed that the region between ^{835}Ala and ^{918}Asp of the EGFR cytoplasmic domain is required for EGFR predimer formation. In contrast to wild-type EGFR ligands, a mutant form of heparin-binding EGF-like growth factor (HB2) did not induce dimerization of the EGFR-EpoR chimeric receptor and therefore failed to activate the chimeric receptor. However, when the dimerization was induced by a monoclonal antibody to EGFR, HB2 could activate the chimeric receptor. These results indicate that EGFR can form a ligand-independent inactive dimer and that receptor dimerization and activation are mechanistically distinct and separable events.

INTRODUCTION

Epidermal growth factor receptor (EGFR), a member of the ErbB family of receptor tyrosine kinases, was the earliest noted growth factor receptor. EGFR is an ~180-kDa transmembrane glycoprotein consisting of an extracellular domain containing two cysteine-rich regions, a single transmembrane domain, and an intracellular domain. EGFR has several ligands with similar structures, including EGF, transforming growth factor α, heparin-binding EGF-like growth factor (HB-EGF), amphiregulin, betacellulin, and epiregulin (Marquart *et al.*, 1984; Shoyab *et al.*, 1989; Higashiyama *et al.*, 1991; Shing *et al.*, 1993; Toyoda *et al.*, 1995). The first step in EGFR activation is receptor dimer formation. EGF family molecules activate an EGFR homodimer and an EGFR heterodimer with other ErbB receptors (Tzahar and Yarden, 1998). Dimerized EGFR induces autophosphorylation of tyrosine residues in the carboxyl terminal of EGFR by its own kinase domain. The resulting phosphorylated tyrosine residues serve as binding sites for molecules containing Src homology 2 domains and initiate intracellular signaling cascades linked to versatile cellular responses, including regulation of gene expression.

Although dimerization and autophosphorylation are the critical events in the activation of EGFR (Yarden and Schlessinger, 1987a,b), the precise mechanisms underlying these events have not been fully elucidated. EGF-induced dimerization of EGFR has been demonstrated in a number of studies, many of which made use of covalent cross-linking agents (Cochet *et al.*, 1988; Lax *et al.*, 1988; Lax *et al.*, 1989; Tanner and Kyte, 1999). Circular dichroism analysis and steady-state fluorescence measurements show that EGF induces a conformational change in the EGFR ectodomain (Greenfield *et al.*, 1989), which may be the basis of EGFR activation. Electron microscopy shows that the ligand not

Article published online ahead of print. Mol. Biol. Cell 10.1091/mbc.01–08–0411. Article and publication date are at www.molbiolcell.org/cgi/doi/10.1091/mbc.01–08–0411.

‡ Corresponding author. E-mail address: emekada@biken.osaka-u.ac.jp.

Abbreviations used: EGF, epidermal growth factor; EGFR, EGF receptor; FCS, fetal calf serum; HB-EGF, heparin-binding EGF-like growth factor; mAb, monoclonal antibody; proHB-EGF, membrane-anchored form of HB-EGF.

only induces a conformational change of the soluble form of EGFR but also stimulates its oligomerization (Lax *et al.*, 1991). Small-angle x-ray scattering assays and isothermal titration calorimetry suggest that the stoichiometry of the ligand binding to soluble EGFR is 2:2 (Lemmon *et al.*, 1997). Dimerization of EGFR and activation of its tyrosine kinase are coincidental events (Canal, 1992); thus, it has been thought that dimerization and activation of EGFR are mechanistically indistinguishable events.

Studies for determining fluorescence resonance energy transfer on fixed A431 cells (Gadella and Jovin, 1995) or single-molecule imaging of EGFR on the surface of living A431 cells (Sako *et al.*, 2000) have implied that preformed dimers of EGFR may exist in intact cell membranes without ligand stimulation. Earlier studies of A431 cells by sucrose density gradient centrifugation or cross-linking also showed that EGFR could form dimers without exogenous ligand stimulation (Boni-Schnetzler and Pilch, 1987; Cochet *et al.*, 1988). However, these studies did not exclude the possibility that EGFR dimers were induced by EGFR ligands provided from the A431 cells themselves (Van de Vijver *et al.*, 1991). Thus, there is no direct evidence to prove the existence of ligand-independent EGFR dimer. We demonstrate here ligand-independent EGFR dimers using Ba/F3 cells and other cell lines. We found that such ligand-independent EGFR dimers were not activated. Comparison of EGFR with an EGFR-erythropoietin receptor (EpoR) chimeric receptor and the use of a HB-EGF mutant indicated that dimer formation and the activation of EGFR are distinguishable processes.

MATERIALS AND METHODS

Reagents and Antibodies

Human recombinant EGF was purchased from Boehringer-Mannheim Co. (Indianapolis, IN). Rabbit anti-EGFR antibody, mouse anti-Cbl monoclonal antibody (mAb), rabbit anti–hemagglutinin-tag antibody, rabbit anti-myc antibody, and rabbit anti–signal transducer and activator of transcription (STAT) 5 were all acquired from Santa Cruz Biotechnology Inc. (Santa Cruz, CA). Mouse anti-EGFR mAb (clone LA1) was purchased from Upstate Biotechnology Inc. (Charlottesville, VA), mouse anti-EGFR mAb (clone EGFR.1) from Neo Markers, horseradish peroxidase (HRP)-conjugated goat anti-mouse immunoglobulin G (IgG) from Zymed Laboratories Inc. (San Francisco, CA), HRP-conjugated goat anti-rabbit IgG from Chemicon International Inc. (Temecula, CA), mouse anti-phosphotyrosine mAb (6D12) from MBL Co (Nagoya, Japan), and mouse anti-Flag mAb (M2) from Sigma Chemical Co. (St. Louis, MO). Rabbit anti–mitogen-activated protein kinase (MAPK) and phospho-MAPK antibody were purchased from New England Biolabs Inc. (Beverly, MA).

Plasmid Construction

A plasmid encoding a glutathione *S*-transferase (GST) fusion protein containing the EGF-like domain of proHB-EGF, corresponding to amino acids 106–149 of human proHB-EGF, was constructed by insertion of the corresponding cDNA sequences of proHB-EGF into the *Eco*RI/*Bam*HI sites of the pGEX-3X plasmid (Pharmacia). The inserted DNA fragment encoding proHB-EGF was prepared by polymerase chain reaction using plasmid pRTHG-1 (Mitamura *et al.*, 1995) as a template. The resulting GST fusion protein, referred to as HB1, encompasses the entire EGF-like domain. Next, HB2, a GST fusion protein containing a mutated EGF-like domain of proHB-EGF, was produced: The coding sequence of proHB-EGF cDNA was mutated from ^{379}CGGAAA to CTTTCA and from ^{388}AAG to GAC. These substitutions resulted in amino acid alterations from ^{110}Arg-^{111}Lys to Leu-Ser and ^{113}Lys to Asp. cDNA of the resulting mutant proHB-EGF, corresponding to amino acids 106–149 and containing the above substitutions, was inserted into the *Eco*RI/*Bam*HI sites of the pGEX-3X plasmid. Truncated EGFR mutants were constructed: pRc/CMV-HA was constructed by the insertion of a DNA fragment encoding the HA-tag epitope into the *Xba*I site of pRc/CMV (Invitrogen, San Diego, CA). Deletion of EGFR was generated by polymerase chain reaction using pTJNEO-EGFR (Gotoh *et al.*, 1992) as the template, and synthesized products were inserted between the *Hin*dIII and *Xba*I sites of pRc/CMV-HA. The sequence of each EGFR mutant was confirmed by sequence analysis.

Purification of GST Fusion Protein

The GST fusion proteins were purified with glutathione Sepharose 4B (Pharmacia, Piscataway, NJ) according to the manufacturer's instructions. GST-HB1 and GST-HB2, eluted from glutathione Sepharose, were dialyzed against HEPES-buffered saline (20 mM HEPES, 150 mM NaCl, pH 7.2) for use in the following experiments. Protein concentrations were determined by the Bradford method using BSA as a standard.

Cell Culture and Transfection

Ba/F3 cells were cultured in RPMI 1640 medium containing 10% fetal calf serum (FCS) and 5% WEHI-3 cell-conditioned medium as a source of interleukin 3 (IL-3). Stable transformants of Ba/F3 cells expressing EGFR or EGFR-EpoR were obtained by selection in medium containing G418 as previously described (Iwamoto *et al.*, 1999). COS-7 cells were maintained in DMEM with 10% FCS. Chinese hamster ovary (CHO) cells were cultured in Ham's F12 medium with 10% FCS. Transfection was carried out by electroporation (Gene Pulser, Bio-Rad, Richmond, CA) according to the manufacturer's instructions.

Treatment with EGF Ligands

Before cross-linking and coimmunoprecipitation assays, cells indicated were incubated with 100 nM of EGF or the recombinant forms of HB-EGF for 3 min, washed with PBS, and then used for further analysis.

Chemical Cross-linking

Chemical cross-linking was carried out as described previously, with minor modifications (Iwamoto *et al.*, 1994). Briefly, the cells were washed with PBS (137 mM NaCl, 0.67 mM KCl, 8 mM Na_2HPO_4, 1.4 mM KH_2PO_4) three times and incubated for 30 min at 4°C with 1 mM dithiobis-(sulfosuccinimdylpropionate) (DTSSP) (Pierce Chemical Co., Rockford, IL) in PBS, followed by washing three times with Tris-buffered saline (TBS) (20 mM Tris-HCl, 100 mM NaCl, pH 7.5) before use in the following studies.

Immunoprecipitation and Immunoblotting

Cells were lysed with 1% Triton X-100 in lysis buffer (0.15 M NaCl, 2 mM EDTA, 1 mM phenylmethylsulfonyl fluoride, 1 mM $NaVO_4$, 50 mM Tris pH 7.5) and then centrifuged for 20 min at 15,000 × *g*. The supernatants were cleared with Sepharose 4B for 1 h and then incubated with primary antibody for 2 h, followed by addition of Sepharose 4B-conjugated secondary antibody. The Sepharose beads were washed three times with lysis buffer and once with deionized water and then were boiled for 5 min in SDS-PAGE sample buffer with or without 50 mM dithiothreitol. Samples were run on SDS-PAGE and electrotransferred to an Immobilon membrane. The membrane was blocked with 3% skim milk in TBS (20 mM Tris, 0.1 M NaCl, pH 7.5) at 37°C for 1 h, then incubated with primary antibody in TBS containing 1% skim milk at room temperature for 1 h. Next, the membrane was washed four times with TTBS (TBS containing 0.05% Tween 20), incubated with HRP-conjugated sec-

ondary antibody, and finally analyzed with an ECL-Western blotting kit (Amersham International plc, Buckinghamshire, England).

DNA Synthesis Assay

Cells were seeded into 24-well plates at a density of 5×10^4 cells/well with or without each EGF ligand in fresh RPMI 1640 medium containing 10% serum, then cultured at 37°C for 24 h and incubated with [^{3}H]thymidine (37 kBq/ml) for 4 h. Cells were harvested, and radioactivity incorporated into DNA was determined as described previously (Iwamoto *et al.*, 1999). The rate of DNA synthesis was expressed as a percentage of the average of the maximum value (40,000 cpm).

Preparation of Fab Fragment

Anti-EGFR mAb (EGFR.1), 1 mg/ml, was incubated with papain (0.1 mg/ml) in PBS at 37°C for 18 h, at which point iodoacetamide (30 mM) was added to stop the reaction. The mixture was dialyzed in PBS at 4°C for 12 h and then purified with goat antimouse IgG Fc antibody conjugated to Sepharose 4B. The size of the Fab fragment was checked by SDS-PAGE, and the Fab concentration was determined by measuring absorbance at 280 nm.

RESULTS

EGF Receptor Exists as an Inactive Dimer without Ligand

Ba/F3 cells are an IL-3–dependent preB-lymphocyte cell line and do not express endogenous murine EGFR, ErbB2, and ErbB4. Although the expression of the detectable amount of ErbB3 transcript was reported (Riese *et al.*, 1995), we did not detect ErbB3 in this cell line at the protein level. BE cells (Ba/F3 cells expressing EGFR), which were generated by transfection of Ba/F3 cells with vectors encoding human EGFR, can respond to and proliferate with EGF and other EGFR ligands. In the absence of IL-3, BE cells can proliferate in an EGFR ligand-dependent manner. Therefore, this cell line allows EGFR activation to be monitored precisely by measuring cell proliferation.

To examine the oligomeric state of EGFR, we undertook a cross-linking analysis with DTSSP, a membrane-impermeable homobifunctional reagent. BE cells cultured in serum-free medium were preincubated with or without EGF and then treated with DTSSP. The cell lysate was immunoprecipitated with anti-EGFR antibody, followed by SDS-PAGE and Western blotting using an anti-EGFR antibody. In the absence of DTSSP, EGF induces dimerization and activation of EGFR, but the dimers are separated into monomers upon SDS electrophoresis. Therefore, only the monomeric 180-kDa form of EGFR was detected by the anti-EGFR antibody (Figure 1A). When EGF-stimulated BE cells were treated with DTSSP, a 360-kDa polypeptide, corresponding to the size of the EGFR dimer, was detected by the anti-EGFR antibody in addition to the 180-kDa EGFR monomer. It should be noted that this 360-kDa molecule was observed in samples from unstimulated BE cells treated with DTSSP. Neither the 360-kDa nor 180-kDa bands were observed when Ba/F3 cells that did not express EGFR were treated with DTSSP (data not shown), thus excluding the possibility of a nonspecific cross-reaction of the anti-EGFR antibody with polypeptides unrelated to EGFR.

To obtain further evidence that the 360-kDa band represents EGFR homodimers, we performed a cross-linking

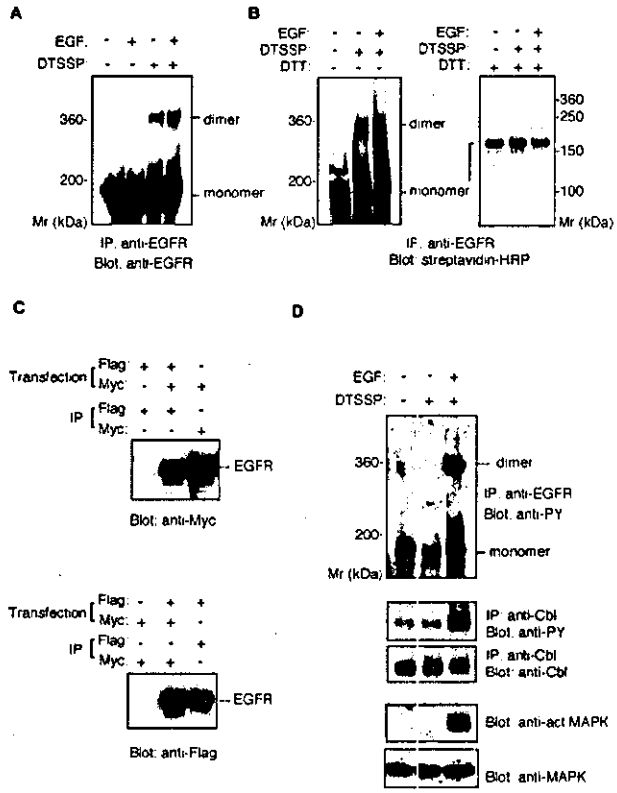

Figure 1. Ligand-independent preformed dimer of EGFR in BE cells. (A) Cross-linking assay of the EGFR dimer. BE cells were preincubated with or without EGF, then treated with DTSSP. The cell lysates were precipitated with rabbit anti-EGFR antibody. Precipitated material was separated by 4% SDS-PAGE in the absence of reducing agents and detected by immunoblot with anti-EGFR mAb. (B) Cross-linking of surface-biotinylated EGFR. BE cells were biotinylated with sulfo-*N*-hydroxysulfosuccinimide-biotin, incubated with or without EGF, and then treated with DTSSP. The cell lysates were precipitated with anti-EGFR polyclonal antibody. Precipitated material was separated by SDS-PAGE in the presence or absence of 5 mM dithiothreitol and detected by immunoblot with streptavidin-HRP. (C) Coimmunoprecipitation assay of epitope-tagged EGFR. COS cells were cotransfected with plasmids encoding EGFR-myc and EGFR-Flag or transfected with either one of the plasmids alone. The transfected cells were lysed and the cell lysates immunoprecipitated by rabbit anti-myc antibody or anti-Flag mAb. The precipitated materials were separated by 7% SDS-PAGE, transferred to an Immobilon membrane, and blotted with rabbit anti- myc or anti-Flag mAb. (D) Phosphorylation of EGFR, Cbl, and MAP kinase. BE cell lysates were immunoprecipitated with anti-EGFR polyclonal antibody or anti-Cbl antibody. Precipitated materials were subjected by SDS-PAGE and Western blotting using anti-phosphotyrosine mAb or anti-Cbl antibody. MAP kinase and phosphorylated MAP kinase were detected from the cell lysate by Western blotting using anti-MAP kinase or anti-phosphorylated MAP kinase antibody.

analysis using cells whose surface was prelabeled by the biotinylation reagent sulfo-*N*-hydroxysulfosuccinimide–biotin. After cross-linking with DTSSP, the cell lysate was immunoprecipitated with anti-EGFR antibody, and the precipitated material was subjected to SDS-PAGE in the pres-

ence or absence of a reducing agent. Because DTSSP is cleaved in the presence of a reducing agent, cross-linked proteins would be split into their monomeric forms. In the absence of the reducing agent, the 360-kDa and 180-kDa polypeptides were detected by Western blotting with streptavidin-HRP, whereas only the 180-kDa polypeptide was detected in the presence of the reducing agent (Figure 1B), indicating that the 360-kDa cross-linked dimers had been reduced to 180-kDa EGFR monomers. BE cells do not express any other ErbB family proteins, excluding the possibility of heterodimer formation of EGFR with other ErbB family receptors.

To confirm the formation of EGFR homodimers, we performed coprecipitation assays using two kinds of epitope-tagged EGFR constructs. EGFR-Flag and EGFR-myc contain Flag and Myc tags, respectively, in the C-terminal region of EGFR. EGFR-Flag and EGFR-myc were cotransfected into COS-7 cells and incubated in serum-free media. The cell lysates were precipitated with anti-Flag antibody, and the precipitated material was analyzed by Western blotting using the anti-Myc antibody, or vice versa. Figure 1C shows that EGFR-myc coprecipitated with the anti-Flag antibody, and EGFR-Flag coprecipitated with anti-Myc antibody, from cell lysates prepared by culturing cells in the absence of EGF ligands. This confirms the ability of EGFR to form homodimers in the absence of ligand stimulation.

The above results indicate that EGFR, or at least some of the EGFR molecules on the cell surface, may exist as dimers in the absence of ligand stimulation. Although it appears that EGFR activation should not be able to occur without EGF binding, our use of BE cells preincubated with serum-free medium 2 h before the cross-linking study led us to explore the activation state of preformed EGFR dimers under serum-free conditions. When EGF-treated BE cells were analyzed by the cross-linking assay, the 360-kDa homodimer and the 180-kDa monomer of EGFR were highly phosphorylated, as demonstrated by an anti-phosphotyrosine antibody (Figure 1D). In EGF-untreated cells, however, both EGFR homodimers and monomers were found to be not highly phosphorylated. Although a weak band of 180 kDa appeared, it was the basal-level phosphorylation of unstimulated EGFR (Figure 1D). Cbl and MAPK, downstream substrates of the EGFR signal, were also unphosphorylated (Figure 1D), supporting the case for an inactive state of EGFR.

Ligand-independent Dimer Formation Requires the Cytoplasmic Domain of EGFR

The EGFR-EpoR chimeric receptor, designated −108 (Iwatsuki *et al.*, 1997), brings together the extracellular and the transmembrane domains of EGFR with part of the cytoplasmic domain of EpoR and is linked to an HA tag at its carboxy terminus. Cells expressing this chimeric receptor proliferate under the influence of EGFR ligands (Ohashi *et al.*, 1994). The chimeric receptor was used to examine whether the cytoplasmic domain of EGFR is required for the predimer formation. Like BE cells, B108 cells, stable transformants of Ba/F3 cells expressing chimeric receptor, can respond and proliferate upon stimulation with EGF and other EGF ligands. B108 cells were preincubated with or without EGF, treated with DTSSP, lysed, and finally analyzed by SDS-PAGE and Western blotting. The monomeric form of the chimeric receptor gives a band of ~120 kDa in SDS gels (Figure 2A). When B108 cells were stimulated with EGF and then treated with the cross-linker DTSSP, a dimer of the chimeric EGFR-EpoR molecule of ~240 kDa was observed in addition to the monomer (Figure 2A). However, unlike wild-type EGFR, dimers of the chimeric receptor were not observed in the absence of EGF stimulation (Figure 2A).

The EGFR-EpoR chimeric receptor was further studied by coimmunoprecipitation experiments. Both wild-type EGFR and the EGFR-EpoR chimeric receptor were transiently expressed in COS-7 cells, which were then treated with or without EGF. The cell lysates were immunoprecipitated for coprecipitation assay with an anti–HA-tag antibody, which recognizes the EGFR-EpoR chimeric receptor, or an anti-EGFR antibody, which specifically recognizes the cytoplasmic domain EGFR and does not bind to the EGFR-EpoR chimeric receptor. When cells were treated with EGF, the EGFR-EpoR chimeric receptor coprecipitated with EGFR and the anti-EGFR antibody, as confirmed by Western blot-

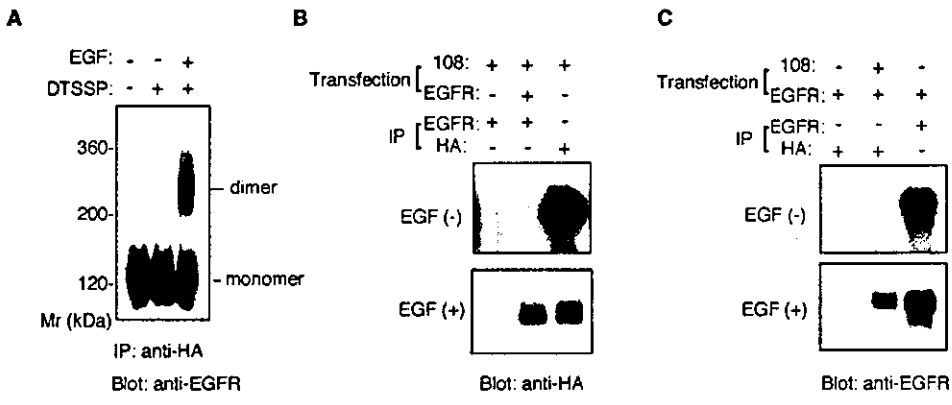

Figure 2. Failure of EGFR-EpoR chimeric receptors to form ligand-independent dimers. (A) Cross-linking analysis of chimeric receptor dimers. B108 cells were preincubated with or without EGF and then treated with DTSSP. The cell lysates were immunoprecipitated with rabbit anti–HA-tag antibody. Precipitated material was separated by 4.5% SDS-PAGE in the absence of reducing agents and detected by immunoblot with mouse anti-EGFR mAb. (B and C) Coimmunoprecipitation assay for the detection of preformed heterodimers of EGFR-EpoR chimeric receptors with EGFR. COS cells were cotransfected with plasmids encoding the EGFR-EpoR chimeric receptor (108) and EGFR or transfected with either of the plasmids alone. The transfected cells were incubated with or without EGF. The cell lysates were immunoprecipitated by rabbit anti-EGFR antibody or rabbit anti–HA-tag antibody. The precipitated materials were separated by SDS-PAGE, transferred to an Immobilon membrane, and blotted with rabbit anti–HA-tag antibody (B) or anti-EGFR antibody (C).

ting using an anti-HA-tag antibody (Figure 2B). However, such coprecipitation of the EGFR-EpoR chimeric receptor was not observed without EGF stimulation (Figure 2B). Similar results were obtained by immunoprecipitation with the anti-HA antibody, in which the coprecipitation of wild-type EGFR was detected by the anti-EGFR antibody (Figure 2C). These results, together with the results of the cross-linking experiments, indicate that the EGFR-EpoR chimeric receptor does not homodimerize in the absence of ligand stimulation and that the cytoplasmic domain of EGFR is required for formation of such predimers.

To confirm the role of the cytoplasmic domain of EGFR in its predimer formation and to narrow down the responsible region, we made a series of truncation mutants of EGFR. The mutants ED1–ED5 possess the protein kinase domain but are lacking parts of the autophosphorylation domain, whereas ED6–ED9 are lacking either part of or all of the kinase and the autophosphorylation domains (Figure 3A). All the EGFR mutants were transiently expressed in CHO cells, and the cross-linking assay was performed. Mutants from ED1 to ED6 formed homodimers without EGF stimulation, whereas ED7, ED8, and ED9 failed to form predimers (Figure 3B). However, in the presence of EGF stimulation, all the truncated EGFR mutants were induced to form homodimers (Figure 3C). Because ED7, ED8, and ED9 are lacking part or all of the kinase domain, these mutants could not generate signals to activate the MAPK pathway on EGF treatment (Figure 3C). These results indicate that the region between ^{835}Ala and ^{918}Asp is important for both EGFR predimer formation and EGFR activation.

EGFR-EpoR Chimeric Receptor and EGFR Show Different Mitogenic Responses

Because EGFR predimer formation and activation require a similar region, it is difficult to use EGFR truncation mutants to study the biological significance of EGFR predimer formation. To further explore the biological significance of preformed EGFR dimers, we studied wild-type EGFR and EGFR-EpoR chimera and compared their physiological reactions to treatment with EGFR ligands. First, we examined the mitogenic response, as measured by the level of DNA synthesis activity, of BE and B108 cells upon stimulation with EGF or related ligands. Figure 4, C and D, show that DNA synthesis in BE and B108 cells is stimulated equally by EGF. Mitogenic responses were also studied for two kinds of recombinant HB-EGF molecules. HB1 is a GST fusion protein of HB-EGF containing only the EGF-like domain of human HB-EGF, whereas HB2 is similar to HB1 but has substitutions of three amino acid residues in the EGF-like domain (Figure 4A). Like EGF, HB1 stimulated DNA synthesis equally in BE and B108 cells. However, HB2 was a less efficient mitogen for B108 cells. HB2 at 3 and 30 nM induced DNA synthesis in BE cells to ~38 and 70% of maximum induction, respectively, but not at all in B108 cells. Fifty times more HB2 was necessary to achieve the same 40% of maximum induction in B108 compared with BE cells.

The number of the EGFR-EpoR chimeric receptors on B108 cells is 2 times less than that of EGFR on BE cells (Figure 4B). To examine whether or not the different mitogenic response of B108 cells to HB2 is a result of the lesser amount of receptor molecules on the cell surface, we isolated another clone of Ba/F3 cells that expresses a smaller amount

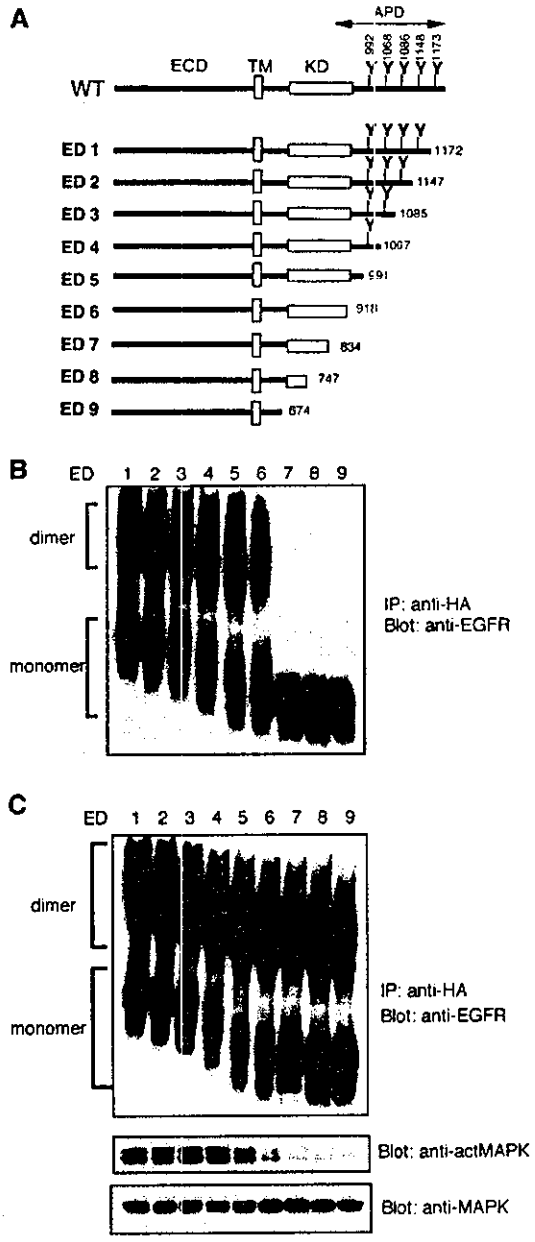

Figure 3. Predimer formation of EGFR mutants. (A) Schematic structure of EGFR mutants. Amino acids are shown as one-letter symbols, and numbers in the figure indicate the number of amino acids from the N-terminus of human EGFR. ECD, extracellular domain; TM, transmembrane domain; KD, kinase domain; APD, autophosphorylation domain; WT, wild-type. (B and C) Cross-linking analysis of EGFR mutants. CHO cells were transfected with plasmids encoding each EGFR mutant. Cells were incubated with (C) or without (B) EGF and then treated with DTSSP. The cell lysates were immunoprecipitated with anti-EGFR mAb. Precipitated material was separated by 4.5% SDS-PAGE in the absence of reducing agents and detected by immunoblot with rabbit anti-HA-tag antibody. MAP kinase and phosphorylated MAP kinase were detected from the cell lysates by Western blotting using anti-MAP kinase or anti-phosphorylated MAP kinase antibody (C).

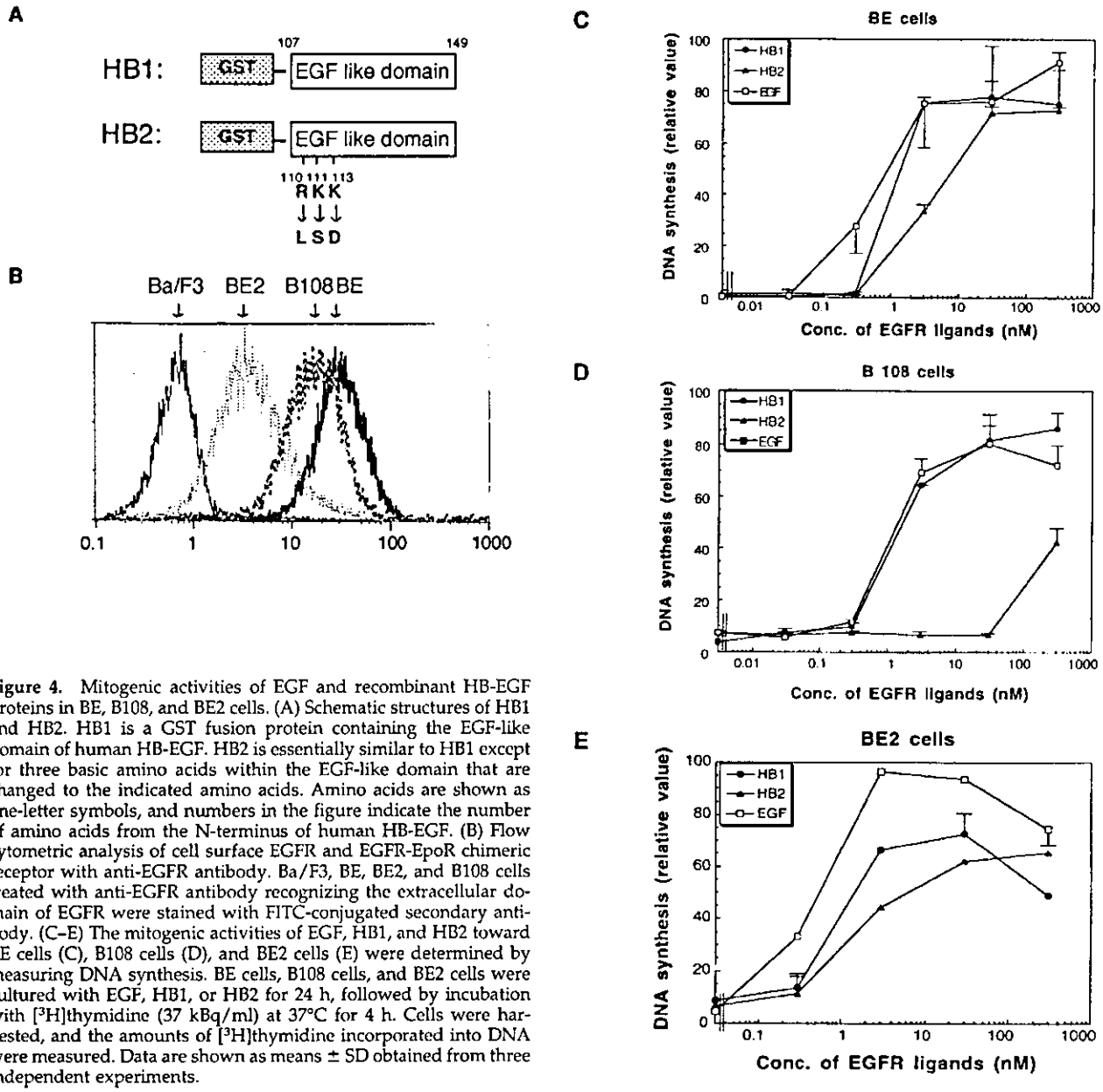

Figure 4. Mitogenic activities of EGF and recombinant HB-EGF proteins in BE, B108, and BE2 cells. (A) Schematic structures of HB1 and HB2. HB1 is a GST fusion protein containing the EGF-like domain of human HB-EGF. HB2 is essentially similar to HB1 except for three basic amino acids within the EGF-like domain that are changed to the indicated amino acids. Amino acids are shown as one-letter symbols, and numbers in the figure indicate the number of amino acids from the N-terminus of human HB-EGF. (B) Flow cytometric analysis of cell surface EGFR and EGFR-EpoR chimeric receptor with anti-EGFR antibody. Ba/F3, BE, BE2, and B108 cells treated with anti-EGFR antibody recognizing the extracellular domain of EGFR were stained with FITC-conjugated secondary antibody. (C–E) The mitogenic activities of EGF, HB1, and HB2 toward BE cells (C), B108 cells (D), and BE2 cells (E) were determined by measuring DNA synthesis. BE cells, B108 cells, and BE2 cells were cultured with EGF, HB1, or HB2 for 24 h, followed by incubation with [^{3}H]thymidine (37 kBq/ml) at 37°C for 4 h. Cells were harvested, and the amounts of [^{3}H]thymidine incorporated into DNA were measured. Data are shown as means ± SD obtained from three independent experiments.

of EGFR. As shown in Figure 4B, BE2 cells express EGFR, but the number of EGFRs on the cell surface is ~9 times less than that of BE cells. BE2 cells showed a mitogenic response to HB2 similar to that of HB1 (Figure 4E), also as in BE cells, indicating that the different mitogenic response of B108 cells to HB2 is not caused by the smaller amounts of receptor molecules on the cell surface.

Defect of HB2 in the Dimerization of EGFR-EpoR Chimeric Receptor

We have shown in this study that the wild-type EGFR, but not the EGFR-EpoR chimera, forms homodimers even in the absence of EGFR ligands. We explored whether the decreased mitogenic response of B108 cells to HB2, compared with that of BE cells, is related to their inability to form dimers in the absence of ligand. Cross-linking analysis by DTSSP indicated that, whereas homodimer formation in BE cells is EGFR ligand-independent, phosphorylation of the EGFR homodimer and the subsequent activation of downstream signaling molecules are ligand-dependent (Figure 1). Like EGF and HB1, HB2 stimulated phosphorylation of the EGFR homodimer and MAPK in BE cells (Figure 5A). In the case of the EGFR-EpoR chimeric receptor, treatment of B108 cells with EGF or HB1 resulted in dimer formation and the activation of MAPK and STAT5, the substrates downstream